Koninklijk Nederlands Meteorologisch Instituut
Ministerie van Verkeer en Waterstaat

Deltares
Enabling Delta Life

Evaluation of HARMONIE simulations for 16 historical storms

Contribution to WP 1 of the WTI2017-HB Wind Modelling Project

Final

July 2013

Evaluation of HARMONIE simulations for 16 historical storms

Contribution to WP 1 of the WTI 2017 Wind Modelling Project

Peter Baas
Royal Netherlands Meteorological Institute

July 22, 2013

Abstract

For the derivation of the Hydraulic Boundary Conditions (HBCs), information on extreme winds over open-water areas is required. To this end, a new method is developed that will answer the need for a description of both the strength and the space- and time-characteristics of extreme storms. The method relies on using high-resolution atmospheric model simulations rather than on using spatial interpolation of sparse point measurements of wind speed. The HARMONIE model, which has a grid spacing of 2.5 km, has been selected to perform the simulations.

Following the model setup described by Van den Brink *et al.* (2013), this report presents a verification of HARMONIE simulation of 16 historical storms that were recommended by Groen and Caires (2011). Based on a verification with observations, we conclude that the wind fields produced by the model are realistic. Over sea, modelled wind speeds show a positive bias of about 0.5 m/s; for most stations the rms error is between 1.5 and 2.0 m/s. The bias in wind direction is a few degrees, the rms error is order 10° for winds of 8Bft and higher.

Temporal correlation between modelled and observed wind speed is 0.95 over sea. Spatial characteristics are generally well-captured. Spatial correlation between observations valid at the same time amounts 0.87 on average. HARMONIE represents spatial gradients between a selection of stations in 10-m wind speed and surface pressure rather well. Wind patterns over Lake IJssel are accurately reproduced by the model, including the impact of stability on the near-surface wind speed. It is demonstrated that for high wind speeds stability effects leave the vertical wind speed ratio relatively unaffected, while the water/land ratio changes significantly.

Given the results of the validation, the HARMONIE model set-up used for the simulation of the 16 validated storm periods will also be used for the long-term HARMONIE simulations.

Keywords
HARMONIE, model evaluation, extreme wind, stability

Executive Summary

General

According to the Dutch Water Act (Waterwet, 2009) the safety of the Dutch primary water defences must be assessed periodically. The water defences must offer protection against water levels and wave conditions at normative conditions, known as Hydraulic Boundary Conditions (HBCs). To obtain reliable HBCs, accurate wind fields are required. To ensure that the quality of the HBCs will meet future needs, Rijkswaterstaat has funded a long-term R&D project, WTI2017-Hydraulics Loads. The goal of the WTI2017-Wind Modelling subproject is to improve on existing methodologies by making use of model simulations.

Problem statement and goals

For the determination of the HBCs, information on open-water surface winds is required for driving hydrodynamic models. The presently used wind fields are based on spatial interpolation of point measurements from the network of KNMI wind stations. Unfortunately, most of the measurement locations are located over land. Although the current interpolation methods to convert land-based observations to open-water winds are based on well-established theories, contradictory results were obtained for extreme winds (e.g. Caires *et al.*, 2009).

Given the limitations of the applied method, the Hydraulic Review Team advised the use of numerical models instead. It is anticipated that in this way fewer assumptions are needed, and that more physically realistic space-time patterns can be obtained. Recently, the WTI2017-Wind Modelling project was initiated to set up a new method based on high-resolution atmospheric model simulations for estimating extreme surface wind fields. To perform the simulations, the HARMONIE model (www.hirlam.org) was selected. Since 2012 HARMONIE has been used by KNMI for high-resolution weather forecasting. It is run at a resolution of 2.5 km grid size. The aim of this report is to establish how well the high-resolution atmospheric model (i.c. HARMONIE) is capable of simulating realistic (open water) wind fields, including their variations in time and space.

Approach

To gain confidence in the high-resolution wind fields produced by the model, this report evaluates hindcasts of 16 historical storms, that were recommended by Groen and Caires (2011), against observations. The storms have been simulated following the model set-up as described by Van den Brink *et al.* (2013). Results are compared with station observations from KNMI and with satellite winds derived from a scatterometer. In particular, the models ability to represent land-water transitions and the influence of atmospheric stability on the wind field are discussed.

Conclusions

Based on the verification with observations, we conclude that the wind fields produced by the model are realistic. Temporal and spatial characteristics of the storms are generally well-captured. Discrepancies with observations are largest for small storm depressions, which develop explosively and that pass close to The Netherlands

Over sea, modelled wind speeds show a positive bias of about 0.5 m/s. For most stations, the rms error is between 1.5 and 2.0 m/s. For wind speeds over 17.2 m/s (8 Bft or higher) these values hardly change. The bias in wind direction is a few degrees, rms scores range from 15° when all data are taken into account to order 10° for winds of 8Bft and higher. These numbers are rather similar to those derived in operation practice. Note that the observational error is about 1 m/s in the wind speed and 10° in wind direction. Bias and rms error scores based on satellite winds over open water from Quikscat agree with scores derived from station observations.

Over land, the wind speed bias is mostly close to zero with rms errors between 1.0 and 1.5 m/s. However, for wind speeds over 8 Bft generally a negative bias of about 2 m/s is identified with rms errors varying from 1.5 to 4 m/s. Temporal correlation between modelled and observed wind speed is 0.95 over sea. Spatial characteristics are generally well-captured. Spatial correlation between observations valid at the same time amounts 0.87 on average. HARMONIE represents spatial gradients between a selection of stations in 10-m wind speed and surface pressure rather well. Wind patterns over Lake IJssel are accurately reproduced by the model, including the impact of stability on the near-surface wind speed. It is demonstrated that for high wind speeds stability effects leave the vertical wind speed ratio relatively unaffected, while the water/land ratio changes significantly.

Given the results of the validation, the HARMONIE model set-up used for the simulation of the 16 validated storm periods will also be used for the long-term HARMONIE simulations. Any recommendations resulting from the validation in terms of hydrodynamic loads are not to be made in terms of adjusting the HARMONIE model set-up, but rather in terms of post-processing of the HARMONIE data.

Follow-up steps

To establish the value of the high-resolution model for the determination of the HBCs in more detail, simulations with hydrodynamic models must be performed. This will demonstrate the added value of the high-resolution model in terms of calculated surges and wave characteristics. To be able to derive extreme winds with a return period of 10000 years, all storm periods in the ERA-Interim period (1979-2010) will be simulated with HARMONIE. In total, we have computing capacity to simulate roughly 20% of the ERA-Interim period. The long-term dataset of simulations will also be used to determine if any post-processing of the HARMONIE wind fields is required.

Contents

1 Introduction **6**
1.1 WTI 2017 6
1.2 WTI2017-Wind Modelling 7
1.3 Motivation 7
1.4 Objectives 8
1.5 Overview of simulated storms 8
1.6 Criteria 9
1.7 Report outline *10*
1.8 Acknowledgements 10

2 Measurement data **11**
2.1 KNMI stations 11
2.1.1 Overview of network 11
2.1.2 Data processing 12
2.1.3 Benschop correction 12
2.1.4 Quality aspects 14
2.2 RWS stations at Lake Ijssel 15
2.3 Scatterometer 15

3 Model characteristics and evaluation strategy **17**
3.1 Set-up of the simulations 17
3.2 Comparing model grid boxes with point observations 18
3.3 Temporal resolution of model output and observations 20
3.4 Representation of atmospheric stability 22
3.4.1 Impact of enhanced sea surface temperature 22
3.4.2 Comparison with tall mast observations 25

4 Results **27**
4.1 Evaluation of wind and pressure fields 27
4.1.1 Wind distributions 27
4.1.2 Temporal evolution 28
4.1.2.1 Metrics of complete hindcast periods 28
4.1.2.2 Storm dependent scores 32
4.1.2.3 Modelled and observed rate of change of wind speed 33
4.1.3 Spatial characteristics (based on station observations) 35
4.1.3.1 Metrics of spatial correspondence 35
4.1.3.2 Spatial gradients in model and observations 36
4.1.4 Comparison with scatterometer winds 40
4.2 Wind patterns over Lake IJssel 41
4.3 Surface stress 44
4.4 Comparison between HARMONIE and ERA-Interim 46

5 Conclusions and follow-up steps **48**
5.1 Conclusions 48
5.2 Follow-up steps 49

References **50**

1 Introduction

In compliance with the Dutch Water Act (Waterwet, 2009) the strength of the Dutch primary water defences must be assessed periodically[1] for the required level of protection, which, depending on the area, may vary from 250 to 10000 year loads; see Figure 1.1. These loads are determined on the basis of Hydraulic Boundary Conditions (HBC).

Figure 1.1. The safety standard of the Dutch primary water defences.

1.1 WTI 2017

With the aim of delivering legal assessment instruments for the fourth assessment period, starting in 2017, Rijkswaterstaat – Dienst Water, Verkeer en Leefomgeving is funding the long-term project WTI 2017. The WTI (”Wettelijk Toets Instrumentarium”: legal assessment instruments) project provides the HBC and other necessary instruments for the assessment of the primary sea defences. Insights have changed over the years and many developments have triggered improvements to the instrumentation. The research project Strengths and Loads of Water Defences (”Sterkte en Belastingen Waterkeringen”, SBW) started ten years ago with the aim to provide expertise and instruments for WTI.

At the moment, extreme wind fields required for the determination of the HBCs are based on point statistics of KNMI stations. For each water system, the methodology is described in De Waal (2010) and Lopez de la Cruz *et al.* (2010). The methods are mostly ad-hoc and for

[1] Previous assessments took place in 1996, 2001 and 2006. The date of the next assessment is 2017 and for the period after 2017 the assessment will be on a continuous basis.

many water systems the created fields are uniform or with a fixed spatial gradient. This is unrealistic. For some water systems, time evolutions are accounted for, but these are strongly schematized. However, for many failure mechanisms the temporal and spatial variations of the storm are important. In fact, the majority of the knowledge gaps in the various techniques and methods that are needed to derive the HBCs are “time” and “space” dimension related.

1.2 WTI2017-Wind Modelling

To obtain reliable HBCs, accurate (especially open-water) wind fields are required. Recently, following the advice of the Hydraulic Review Team, the KNMI-Deltares ”WTI2017-Wind Modelling” project was initiated to set up a new method based on high-resolution atmospheric model simulations for estimating extreme surface wind fields. It is anticipated that in this way fewer assumptions are needed, and that more physically realistic space-time patterns can be obtained. Moreover, especially above open water sufficiently long time series of wind speed are virtually absent; a problem that does not occur when output from an atmospheric model is used (cf. Tammelin *et al.*, 2011). Also problems related to data inhomogeneities like station displacement, changes in measurement technique, and periods with missing data are avoided (Weisse *et al.*, 2009). An overview of the WTI2017-Wind Modelling project is given in Groeneweg *et al.* (2011; 2012a) and will not be reproduced here.

Utilizing atmospheric model output instead of observations is of no use if the quality of the model data is insufficient. Therefore, as part of the WTI2017-Wind Modelling project, Groen and Caires (2011) selected and described 17 storm periods that will serve as test events to analyze whether the model is capable of simulating extreme wind events. The HARMONIE model (Seity *et al.*, 2011), which has a grid-spacing of 2.5 km, was selected to perform the simulations. In an interim report, Baas and De Waal (2012) described the first results of HARMONIE based on two of the selected storm periods using a preliminary model set-up. Based on, among others, recommendations that were made in this report, Van den Brink *et al.* (2013) documented the model configuration that will be used in the project. The present report is specifically concerned with results of the Work Package 1 (WP1), as described in Groeneweg *et al.* (2011), milestone ”Report specification and results model simulations 16 storms, including temporal and spatial characteristics” as defined in the project overview. (One of the selected storms was left out of the evaluation, see Section 1.5.)

1.3 Motivation

In summary, extreme wind fields based on high-resolution HARMONIE model output will in principle show more realistic spatial and temporal patterns than the wind fields that are currently used in the determination of the HBCs. This facilitates the wish to include time-dependency in the calculations on failure mechanisms. Also for hydraulic loads calculations, taking into account spatial and temporal variations in the wind fields is desired since, for example, rotation of the wind may have a large impact on the attained water levels.

Moreover, although the current interpolation methods to convert land-based observations to open-water winds are based on well-established theories, contradictory results were obtained for extreme winds (e.g. Caires *et al.*, 2009).

Before HARMONIE wind fields can be used as a basis for estimating extreme winds with return periods of 10000 years (Groeneweg *et al.*, 2012b), an assessment has to be made of the quality of the modelled wind fields in observed extreme conditions. Therefore, the present report provides a comprehensive verification of the model simulations of 16 historical storms against observations. Since most of the knowledge gaps in the various techniques and methods that are needed to derive the HBC are related to the 'time' and 'space' dimension, special emphasis is given to the temporal and spatial characteristics of the storms.

1.4 Objectives

The aim of this report is to establish how well the high-resolution atmospheric model (i.c. HARMONIE) is capable of simulating realistic (open water) wind fields, including their variations in time and space.

Specific objectives of this report include

- To validate simulated wind fields of 16 selected storms against observations, with special focus on the spatial and temporal characteristics of the storms.
- To document the model's ability to represent land-water transitions. Special attention will be given to the representation of Lake IJssel.
- To document the model's ability to capture the influence of atmospheric stability on surface wind fields.
- To identify possible situations in which the model behaves problematically.

1.5 Overview of simulated storms

Using the model configuration described in Van den Brink *et al.* (2013) the 17 storms of the test set described by Groen and Caires (2011) were simulated with HARMONIE. Table 1.1 gives an overview of the selected storms. Apart from large scale characteristics of the storms (prevailing wind direction, dimensions, relevance in terms of hydraulic loads), it indicates the period for which HARMONIE simulations have been performed.

For several reasons we left the 1953 storm out of the model evaluation. For this storm, no ERA-Interim fields are available, so we had to drive HARMONIE with data from the lower quality ERA40 dataset. In a qualitative sense, the HARMONIE simulation of the 1953 storm shows that the model is capable of simulating the storm, but the difference in model setup hampers a quantitative comparison with other storms. From an observational point of view, only five stations with observations are available for this storm. More importantly, the quality of the available observations is uncertain (Verkaik, 2001). Compared to the other storm periods, measuring conditions have changed substantially (e.g. Vlissingen and De Kooy

have been moved several kilometers; instrumentation types have changed; the measuring height in De Bilt was 37.5 m while it is 10 m (1961-1993) or 20 m (after 1993) for other storm periods). For these reasons, no useful comparison could be made between the 1953 storm and the other storms in the test set.

Table 1.1. Overview of simulated storms (adopted from Groen and Caires (2011), their Table 3.1). Columns show case numbers, dates of the main storm events, the maximum potential wind speed, the number of locations (out of 21) for which the event is ranked in the top-3 in terms of potential wind speed and hydraulic parameters, prevailing wind direction, width of the major wind field, length of the major wind field, displacement of the storm centre in 24 hours, estimated change in the 850 hPa temperature, passage of frontal system. The last two columns indicate the start date and end date of the HARMONIE simulations.

Nr.	Max. wind date	Max. U_p (m/s)	Nr. U_p/ Nr. Hydr. peaks	Sector	Grad. width (° lat)	Field length (° lat)	Track (° lat)	Delta T850 (°C)	Shift (Y/N)	Hindcast start date	Hindcast end date
1	1953 02 01	25.7	not available	NNW	8	20	8	10	Y	1953 01 26	1953 02 04
2	1979 02 14	24.7	1/0	ENE	5	12	5	5	N	1979 02 10	1979 02 17
3	1983 02 01	24.1	1/4	SW-NW	10	13	10	2	Y	1983 01 27	1983 02 04
4	1983 11 27	24.6	7/0	SW-NW	5	20	11	6	Y	1983 11 23	1983 11 29
5	1984 01 14	26.3	4/0	SW-WNW	16	30	16	5	Y	1984 01 10	1984 01 19
6	1989 02 14	19.3	0/5	NW	7	10	10	3	N	1989 02 10	1989 02 17
7	1990 01 25	27.0	17/2	SW	9	25	15	12	Y	1990 01 21	1990 02 03
8	1990 02 26	24.9	4/4	W-NW	20	25	16	5	Y	1990 02 22	1990 03 02
9	1990 12 12	20.4	0/7	S-NW	5	10	11	4	Y	1990 12 07	1990 12 14
10	1993 11 14	22.5	0/5	SW-NW	4	7	8	5	Y	1993 11 10	1993 11 16
11	1994 01 28	19.4	0/6	NW	7	15	11	5–12	N(5)-Y(12)	1994 01 24	1994 01 30
12	1996 02 19	14.5*	0/0	NE	13	25	12	5	Y	1996 02 15	1996 02 22
13	2000 05 28	22.7	0/0	W	10	20	9	7	Y	2000 05 24	2000 05 30
14	2002 10 27	25.7	12/2	SW-NW	10	10	10	10	Y	2002 10 23	2002 10 29
15	2006 11 01	22.1	0/6	NW-W	12	16	11	14	Y	2006 10 28	2006 11 03
16	2007 01 18	23.5	6/0	SSW-NW	6	25	6	2	Y	2007 01 10	2007 01 20
17	2007 11 09	18.7	0/8	NW	6	25	6	5	N	2007 11 05	2007 11 11

1.6 Criteria

The HARMONIE wind fields should meet the following criteria:

- The wind fields should have realistic patterns in time and space. Wind fields that are presently used for the determination of the HBCs are uniform in time and space.
- Bias and rms errors should be comparable to those obtained in operational performance. This seems a sensible criterion, since these models give satisfactory water levels when used to drive hydrodynamic models like WAQUA

1.7 Report outline

Section 2 describes the observations that are used for the model evaluation. A summary of the model set-up is given in Section 3, together with a description of the evaluation strategy and an analysis of how the model represents atmospheric stability. Section 4 describes the results of the evaluation of the modelled wind fields against observations. The conclusions are summarized in Section 5.

1.8 Acknowledgements

I thank my KNMI colleagues Gerrit Burgers, Henk van den Brink, Fred Bosveld and Ine Wijnant for their support, the discussions we had and their constructive comments on this report. Also thanks to Sofia Caires, Hans de Waal en Jacco Groeneweg from Deltares for the fruitful discussions during our KNMI-Deltares progress meetings and for carefully reading earlier versions of this report.

Jur Vogelzang and Ad Stoffelen from the KNMI satellite wind group are acknowledged for the discussions on the use of scatterometer data and for making these data available for a selection of the storms studied in this report.

Douwe Dillingh (Deltares) is acknowledged for reviewing this report.

The Bundesambt für Seeschifffahrt und Hydrographie is acknowledged for providing data from the FINO measurement tower in the North Sea.

2 Measurement data

2.1 KNMI stations

2.1.1 Overview of network and availability

Figure 2.1 shows the locations of the KNMI wind measurement stations in The Netherlands. Most stations are located over land; the open-water stations are predominantly oil-platforms.

Data availability varies between different stations. For each of the 16 storms of the testset, Table 2.1 indicates for which stations data are available. Per storm, the number of available stations increases from 15 in 1979 to over 50 for the most recent storms.

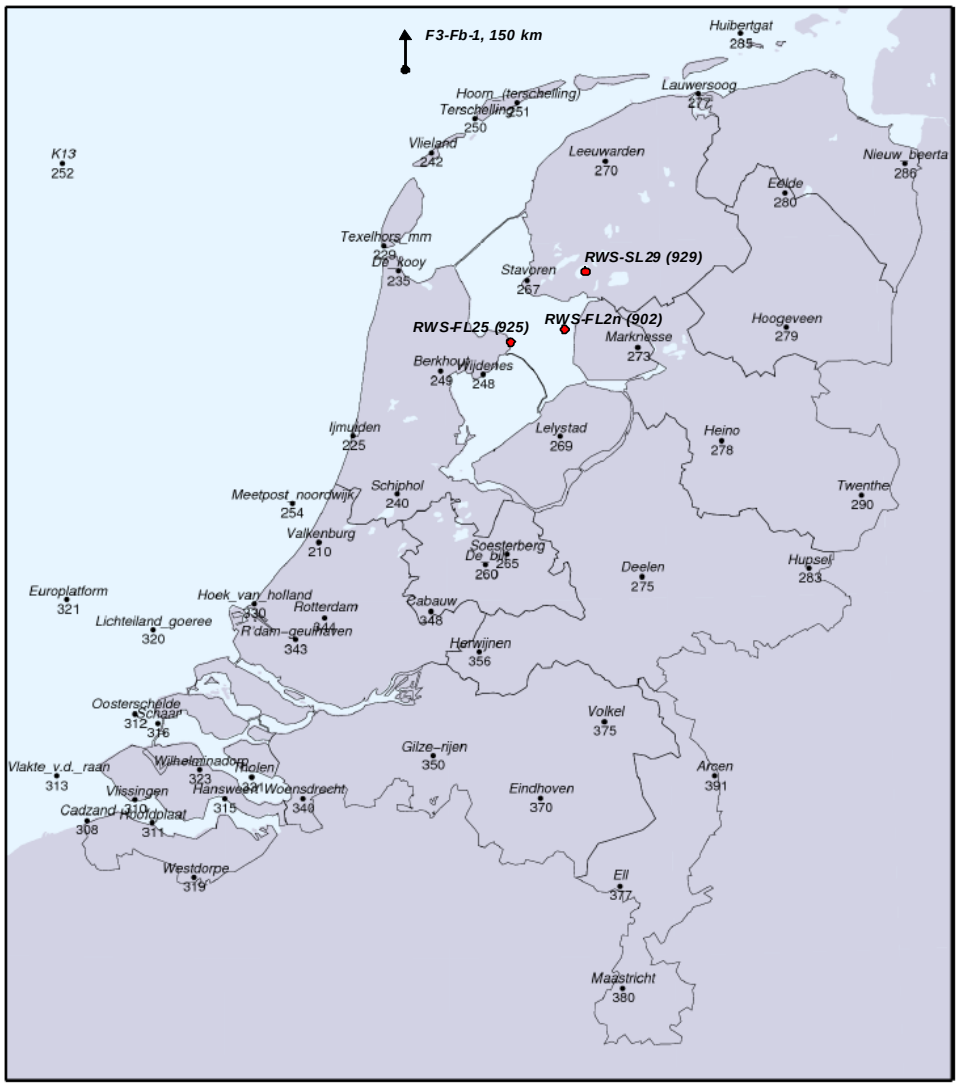

Figure 2.1. Locations of KNMI wind measurement sites. Numbers indicate station codes. Rijkswaterstaat stations are given in red. (From Wever and Groen (2009) with minor modifications.)

2.1.2 Data processing

For the evaluation, data from the KNMI climatological database have been used. Detailed information on measurement systems, procedures and algorithms can be found in the *Handboek Waarnemingen* (Royal Netherlands Meteorological Institute, 2001). For wind speed, the hourly averaged values are archived, together with the average over the last 10 minutes of each hour and the maximum (3 second average) gust that occurred during the hour. For wind direction, the 10-minute average before the whole hour is archived. Since 1995, 10-minute averaged data are available for some stations, since 2003 for almost all stations (Wever and Groen, 2009). The hourly observations are, as a matter of course, subjected to a manual quality control which includes filling of gaps, the 10-minute observations are only subject to standard automated quality control.

Until 1 July 1996, wind speed observations were archived in whole knots (1 knot = 0.514 m/s). Since then, data have been archived in whole m/s. Standard data accuracy is about 1 m/s, but for some non-standard measuring sites, e.g. at oil platforms, and for some periods the accuracy may be lower due to flow distortions (see Verkaik (2001) and references therein).

For temperature, humidity, and pressure the hourly values represent 1-minute averaged values before the whole hour.

2.1.3 Benschop correction

WMO regulations require that wind observations must be performed above short grass (if over land), in open terrain, and at a height of 10 m above the surface. While most measurement locations above land meet these criteria, most stations over sea and some coastal stations measure at a different height. Non-standard measuring heights are indicated in Table 2.1. In accordance with standard KNMI practice, we use the Benschop correction to convert wind speeds from non-standard heights to the 10-m level (Benschop, 1996). The Benschop correction transforms the observed wind at the measurement height to the reference 10-m level using a logarithmic wind profile and the local roughness. Offshore a fixed roughness length of 0.0016 m is used to calculate the Benschop correction. This value originates from applying a Charnock relation with a Charnock constant of 0.032 and a 10-m wind of 15 m/s (Benschop, 1996).

As already indicated by Benschop (1996), application of the Benschop correction is strictly speaking only justified in neutral conditions. Especially in stably stratified conditions large deviations from the assumed logarithmic wind profile may occur. On the other hand, for large wind speeds stability effects are small. This is illustrated in Figure 2.2, which shows the ratio between the wind speed at 73.8 m (measurement height of K13) and 10 m as a function of 10-m wind speed and the air-sea temperature difference. The ratios have been calculated using Monin-Obukhov Similarity Theory. The Benschop correction, valid in neutral conditions, is too high in case of unstable conditions and too low for stable conditions. For wind speeds over 20 m/s the error remains below 3% even for extreme air-sea temperature differences.

Table 2.1. Overview of KNMI observation sites. Columns show station codes, station names, location types (S = open water, C = coast, L = land), measuring heights if different from 10 m, data availability (0 = no data, - = suspicious data, 1 = used data), and the number of storms for which measurements of sufficient quality are available.

				19790214	19830201	19831127	19840114	19890214	19900125	19900226	19901212	19931114	19940128	19960219	20000528	20021027	20061101	20070118	20071109	# storms
391	Arcen	L		0	0	0	0	0	0	0	1	1	1	1	1	1	1	1	1	9
253	AUK-alpha	S	103.3	0	0	1	-	1	-	-	1	1	1	0	1	1	0	0	0	7
380	Beek	L		1	1	1	1	1	1	1	1	1	1	1	1	1	1	1	1	16
249	Berkhout	L		0	0	0	0	0	0	0	0	0	0	0	1	1	1	1	1	5
348	Cabauw	L		0	0	0	0	1	1	1	1	1	1	1	1	1	1	1	1	12
308	Cadzand	C	17.1	1	1	1	1	1	1	1	1	1	1	1	1	1	1	1	1	16
260	De Bilt	L	20	1	1	1	1	1	1	1	1	1	1	1	1	1	1	1	1	16
235	De Kooy	C		1	1	1	1	1	1	1	1	1	1	1	1	1	1	1	1	16
275	Deelen	L		1	1	1	1	1	1	1	1	1	1	1	1	1	1	1	1	16
280	Eelde	L		1	1	1	1	1	1	1	1	1	1	1	1	1	1	1	1	16
370	Eindhoven	L		1	1	1	1	1	1	1	1	1	1	1	1	1	1	1	1	16
377	Ell	L		0	0	0	0	0	0	0	0	0	0	0	1	1	1	1	1	5
321	Europlatform	S	29.1	0	-	-	1	1	1	1	1	1	1	1	1	1	1	1	1	13
206	F16-A	S	75.5	0	0	0	0	0	0	0	0	0	0	0	0	0	0	1	1	2
239	F3	S	59.2	0	0	0	0	0	0	0	0	0	1	1	1	1	1	1	1	7
350	Gilze-Rijen	L		1	1	1	1	1	1	1	1	1	1	1	1	1	1	1	1	16
315	Hansweert	C	16	0	0	0	0	0	0	0	0	0	0	0	1	1	1	1	1	5
278	Heino	L		0	0	0	0	0	0	0	0	1	1	1	1	1	1	1	1	8
356	Herwijnen	L		0	0	0	0	0	1	1	1	1	1	1	1	1	1	1	1	11
330	Hoek van Holland	C	16.6	0	1	1	1	1	1	1	1	1	1	1	1	1	1	1	1	15
311	Hoofdplaat	S	16.5	0	0	0	0	0	0	0	0	0	0	0	1	1	1	1	1	5
279	Hoogeveen	L		0	0	0	0	0	1	1	1	1	1	1	1	1	1	1	1	11
251	Hoorn Terschelling	C		0	0	0	0	0	0	0	0	0	0	1	1	1	1	1	1	6
258	Houtribdijk	S	17.25	0	0	0	0	0	0	0	0	0	0	0	0	0	0	0	1	1
285	Huibertgat	S	18	0	1	1	1	1	1	1	1	1	1	1	1	1	1	1	1	15
283	Hupsel	L		0	0	0	0	0	1	1	1	1	1	1	1	1	1	1	1	11
209	IJmond	S	16.5	0	0	0	0	0	0	0	0	0	0	0	0	1	1	1	1	4
225	IJmuiden	C	18.5	0	1	1	1	1	1	1	1	1	1	1	1	1	1	1	1	15
252	K13	S	73.8	0	-	-	-	1	1	1	1	1	1	1	1	1	1	1	1	12
277	Lauwersoog	C		0	1	1	1	1	1	1	1	1	1	1	1	1	1	1	1	15
270	Leeuwarden	L		0	1	1	1	1	1	1	1	1	1	1	1	1	1	1	1	15
269	Lelystad	C		0	0	0	0	0	1	1	1	1	1	1	1	1	1	1	1	11
320	Lichteiland Goeree	S	38.3	0	-	-	-	1	-	-	1	1	1	1	1	1	1	1	1	10
273	Marknesse	L		0	0	0	0	1	1	1	1	1	1	1	1	1	1	1	1	12
254	Meetpost Noordwijk	S	27.6	0	1	1	1	0	0	1	1	1	1	1	1	1	0	0	0	10
286	Nieuw Beerta	L		0	0	0	0	0	1	1	1	1	1	1	1	1	1	1	1	11
312	Oosterschelde	S	16.5	0	1	1	1	1	1	1	1	1	1	1	1	1	1	1	1	15
343	Rotterdam Geulhaven	L		0	1	1	1	1	1	1	1	1	1	1	1	1	1	1	1	15
902	RWS-FL2	S		0	0	0	0	0	0	0	0	0	0	0	0	0	1	1	0	3
926	RWS-FL26	S		0	0	0	0	0	0	0	0	0	0	0	0	1	1	1	0	3
937	RWS-FL37	S		0	0	0	0	0	0	0	0	0	0	0	0	0	1	1	0	2
929	RWS-SL29	S		0	0	0	0	0	0	0	0	0	0	0	1	1	1	1	0	4
316	Schaar	C	16.5	0	1	1	1	1	1	1	1	1	1	1	1	1	1	1	1	15
240	Schiphol	L		1	1	1	1	1	1	1	1	1	1	1	1	1	1	1	1	16
265	Soesterberg	L		1	1	1	1	1	1	1	1	1	1	1	1	1	1	1	1	16
324	Stavenisse	C	16.5	0	0	0	0	0	0	0	0	0	0	0	1	1	0	1	1	4
267	Stavoren-AWS	C		0	0	0	0	0	0	0	1	1	1	1	1	1	1	1	1	9
229	Texelhors	C		-	1	1	1	1	1	1	1	1	1	1	0	1	1	1	1	14
331	Tholen	C	16.5	0	1	1	1	1	1	1	1	1	1	1	1	1	1	1	1	15
290	Twenthe	L		1	1	1	1	1	1	1	1	1	1	1	1	1	1	1	1	16
210	Valkenburg	C		1	1	1	1	1	1	1	1	1	1	1	1	1	1	1	1	16
313	Vlakte van de Raan	S	16.5	0	0	0	0	0	0	0	0	0	0	0	1	1	1	1	1	5
242	Vlieland	C		0	1	1	1	1	0	0	0	0	0	1	1	1	1	1	1	10
310	Vlissingen	C	27	1	1	1	1	1	1	1	1	1	1	1	1	1	1	1	1	16
375	Volkel	L		1	1	1	1	1	1	1	1	1	1	1	1	1	1	1	1	16
248	Wijdenes	C		0	0	0	0	0	0	0	0	0	0	1	1	1	1	1	1	6
323	Wilhelminadorp	C		0	0	0	0	0	1	1	1	1	1	1	1	1	1	1	1	11
340	Woensdrecht	L		0	0	0	0	0	0	0	0	0	0	1	1	1	1	1	1	6
344	Zestienhoven	L		1	1	1	1	1	1	1	1	1	1	1	1	1	1	1	1	16
	# stations per storm			15	27	28	28	32	35	36	40	41	42	45	52	56	54	56	53	

As an example, the right panel of Figure 2.2 gives the modelled 10-m wind speed and the air-sea temperature differences from 23 Jan – 4 Feb 1990. The warm sector of the storm depression of the 25 Jan 1990 storm depression is known for its high air-sea temperature difference and associated stably stratified conditions. Comparison of the two panels in figure 2.2 shows that even in these conditions application of the Benschop correction introduces only small errors. The modelled air and water temperatures are very similar to the observed values (maximum observed air temperature was 11.2°C with a water temperature of 8.1°C [2])

We conclude that for our purposes application of the Benschop correction is justified. Associated errors are comparable in size to the errors in the observations.

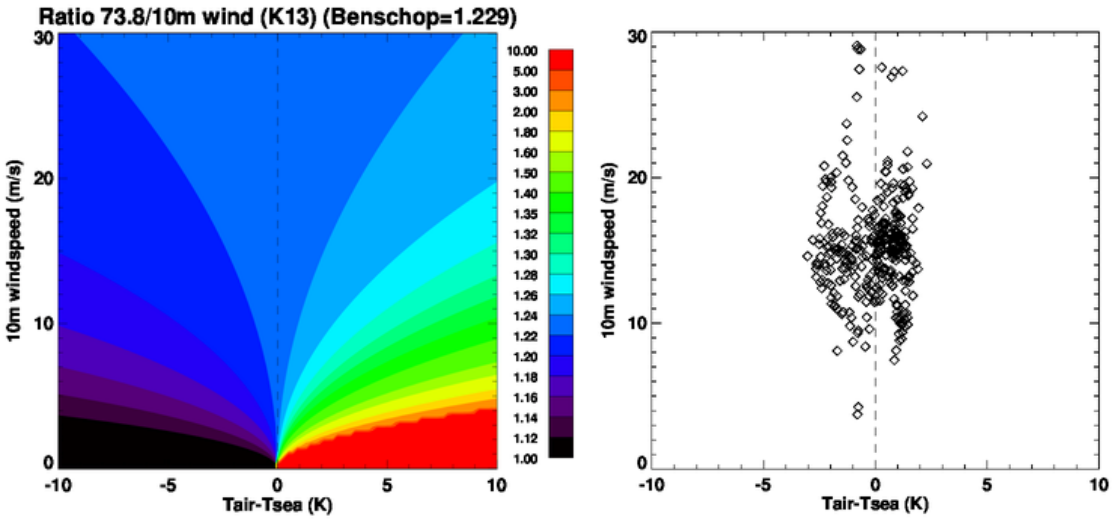

Figure 2.2. Wind speed ratio between 73.8 and 10 m height as a function of 10-m wind speed and the air-sea temperature difference (left). Modelled wind speed versus modelled air-sea temperature difference for the location K13 for 23 Jan – 4 Feb 1990 (right).

2.1.4 Quality aspects

For some storms and for some stations a suspicious mismatch between model data and observations was detected. For instance, Figure 2.3 shows time series of the 10-m wind speed for 14 Jan 1984 for K13 and Texelhors. The clear positive bias of about 4 m/s for K13 persists for the entire 10-day hindcast for this storm. Such a large and persistent bias is absent for surrounding stations such as Texelhors, IJmuiden, Meetpost Noordwijk and Oosterschelde, which suggests that there is something wrong with the observations at K13. A similar bias is apparent for the ERA-Interim fields that are used to initialize HARMONIE. Information from different sources confirms that in this case the observations are suspicious. For example, Verkaik (2001), who inventoried the history of most KNMI wind speed measurements, found unexplainable jumps in the yearly average wind speed at K13 in the

[2] Water temperature at Europlatform for 25 Jan 1990 obtained from http://live.waterbase.nl/waterbase_wns.cfm?taal=nl

1980s. Moreover, there are gaps in the time series where observations are not available and the effect of flow obstructions is clear. Results from Weisse *et al.* (2005) point to a significant underestimation of the observed wind speed in the 1980s. For these reasons, we chose to flag these observations as suspicious and leave them out of the model evaluation.

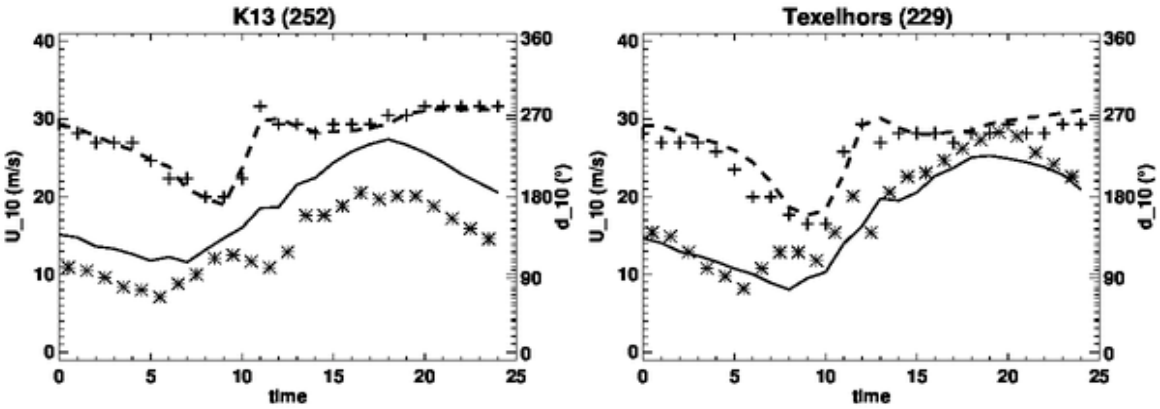

Figure 2.3. Time series of 10-m wind speed (m/s) and direction (°) for 14 Jan 1984 for K13 (left) and Texelhors (right). Solid lines indicate modelled wind speed, dashed lines modelled wind direction. Crosses indicate observed wind speed, plusses indicate observed wind direction.

Comparable long-lasting biases are found for some other platforms for storms in the 1980s. This is in line with the findings of Verkaik (2001), who has great difficulties in indicating the status and quality of the platform observations in this period. Table 2.1 indicates for which storms and stations observations were flagged and ignored in the model evaluation.

2.2 RWS stations at Lake IJssel

In 1997, Rijkswaterstaat (RWS) started an extensive wind and wave measuring campaign in Lake IJssel and Lake Sloten (Bottema, 2007). In this report, we use wind observations of several measuring sites. The locations have been added to Figure 2.1. The measurement height for all these RWS stations is 10 m above the (slightly varying) water level. For consistency with the KNMI stations described above, we use hourly averaged values of wind speed. Detailed information about the measuring instruments can be found in Bottema (2007).

2.3 Scatterometer

From 2000 onwards, over sea we have satellite wind data from the Quikscat scatterometer at our disposal. They have the advantage of an extensive spatial coverage in an area where station observations are rare. A scatterometer measures the electromagnetic radiation scattered back from ocean gravity-capillary waves (Portabella and Stoffelen, 2009). These are the small-scale surface ripples that are directly related to the wind speed. The

backscattered radiation is related to the 10-m wind by a so-called (inverse) Geophysical Model Function (GMF).

Since scatterometers measure only the backscatter of the water surface, no stability information is included. The stability effect is generally small (on average 0.2 m/s, Vogelzang *et al.*, 2011), especially for high wind speeds, and much smaller than other uncertainties in the GMF. For these reasons, we compare the scatterometer wind directly to the real HARMONIE 10-m wind.

We use the Quikscat 25 km product based on a state-of-the-art processing algorithm developed by KNMI. Each Quikscat image is collocated to the HARMONIE wind field from the nearest hour. Each scatterometer point is compared to the average of all HARMONIE grid points over an area of 25x25 km^2. Since scatterometer data can be considered as instantaneous data, no temporal averaging of HARMONIE data (as with the hourly-averaged station observations) is applied. Typically, 2-3 (partial) overpasses over North Sea per day are availabe.

3 Model characteristics and evaluation strategy

In this Section, the model set-up is summarized, the evaluation strategy is explained, and the model's representation of atmospheric stability is discussed.

3.1 Set-up of the simulations

The 16 storms have been simulated using the model set-up that was described in Van den Brink *et al.* (2013). The most essential elements are reproduced here:

- We use HARMONIE version CY37h1.1 (released in June 2012)
- The model is run on a domain with 500x500 grid points and a grid-spacing of 2.5 km. The domain is centred on 54°N 2°E (see Figure 3.1).
- The model time step is 1 minute, the vertical grid consists of 60 levels (the five lowest levels are at 10, 30, 60, 90, 130 m above ground level).
- Output frequency is once per hour.
- Every 6 hours a forecast with a forecast length of 6 h is initialized from the ERA-Interim reanalysis dataset from the ECMWF.
- Longer time series are constructed by combining the +001 to +006 lead-times of the subsequent HARMONIE runs.
- As in Van den Brink *et al.* (2013), and in concord with the default HARMONIE set-up we use the ECUME drag formulation (Weill *et al.*, 2003) over sea and a Charnock formulation ($\alpha = 0.015$) for lakes and rivers. The ECUME formulation is roughly equivalent to a Charnock formulation with $\alpha = 0.020$.

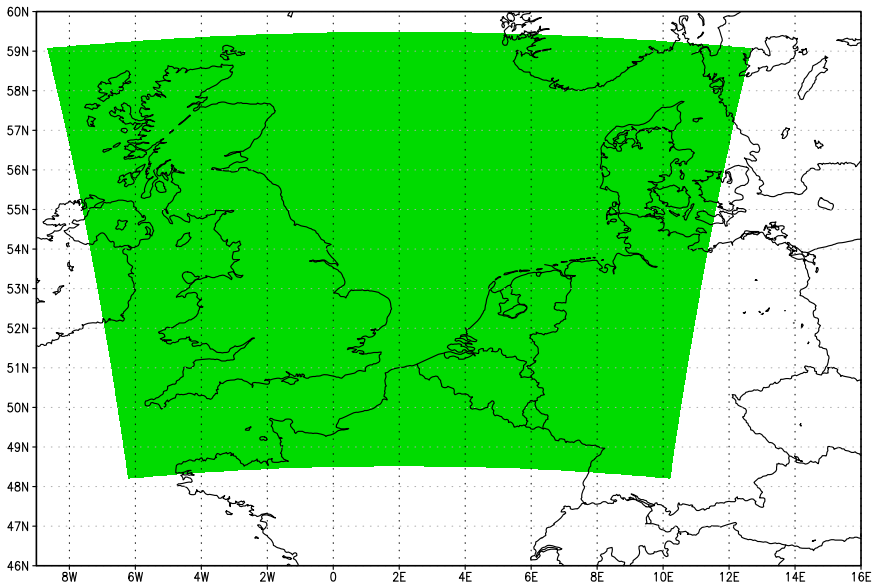

Figure 3.1. HARMONIE domain used for the simulations.

3.2 Comparing model grid boxes with point observations

As demonstrated by various authors (e.g. De Rooy and Kok, 2004; Verkaik, 2006), comparing point observations with model grid values is not trivial, especially not over land. The model applies gridbox-average roughness lengths, which may differ significantly from local values within the gridbox. This is clearly illustrated in Figure 3.2, which shows the HARMONIE grid on top of roughness lengths derived from the LGN3 land use map (which has a resolution of 25 m) for the area around De Bilt: in most gridboxes the roughness length is far from uniform. As WMO regulations require the wind to be measured above short grass in open terrain, it can be anticipated that grid-box averaged model wind speed values will be generally lower than the values observed at the measuring sites.

In coastal areas a slightly different problem occurs. Due to its finite grid size, the model has no sharp coastline. Instead, grid boxes on the actual coastline are composed of a land and a water fraction. This complicates a direct comparison with observations at sites in the coastal zone (Hoek van Holland, Vlissingen): depending on wind direction, these stations may show characteristics of either a land or a water location, whereas the model will show an average behaviour for the grid box where the station is located.

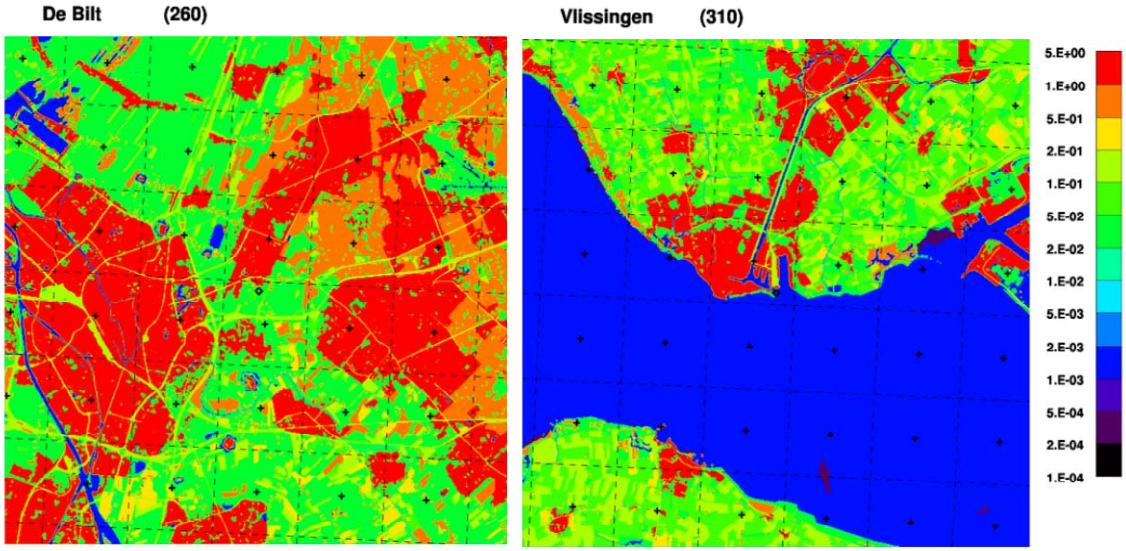

Figure 3.2. LGN3 roughness length map (m) for the areas around De Bilt and Vlissingen. The dashed lines and the plus-signs indicate the 2.5-km HARMONIE grid; the diamonds indicate the station locations.

In this section, we present an objective method which allows for a fair comparison between model grid-boxes and point observations. It is partly based on earlier work of Verkaik (2006) and De Rooy and Kok (2004). First we decide whether the station behaves as a land or a water station using direction dependent roughness information. For each station, observed roughness lengths are derived from exposure correction factors for sectors of 20° based on the standard deviation of the wind speed. If the local upwind roughness length is less than 0.01 m the station is treated as a water station.

In case the station behaves like a water station, the procedure is as follows:

1. Select the grid box with the highest water fraction in a square of 3x3 grid boxes centred on the gridbox in which the observation site is located.
2. If multiple grid boxes with a water fraction of 1 are detected, select the gridbox that is closest to the model upwind direction. For stations located in open water, the nearest gridbox is selected.

In case the station behaves like a land station, the procedure is as follows:

1. Select the gridbox closest to the observation site.
2. Apply physical downscaling. Using the roughness length applied by the model (derived from the 10-m wind speed and the surface stress), the wind speed at a blending height of 60 m above ground level is calculated using a logarithmic wind profile. Next, the 10-m wind used for the model evaluation is calculated using the direction dependent roughness length.

Figure 3.3 illustrates the difference between the procedure described above (left panels) and the method that compares station observations directly to the closest gridbox (right panels) for both a coastal station (Vlissingen) and a land station that is located in complex terrain (Soesterberg). For Vlissingen, the closest gridpoint is located over land and has a high roughness length. The measurement station is located right on the coast. The sigma analysis indicates that the station behaves like a water station for wind directions between 90 and 270°. For these wind directions our algorithm selects the upwind neighbouring gridbox for the evaluation. The large negative bias that can be observed in the ‘closest gridpoint’ approach, is replaced by a small positive bias in our new approach. The downscaling for station Soesterberg changes the difference between model and observations for wind speeds lower than 8 Bft for a significant underestimation to a small overestimation of the model. For higher wind speeds the negative bias is reduced by about 50%.

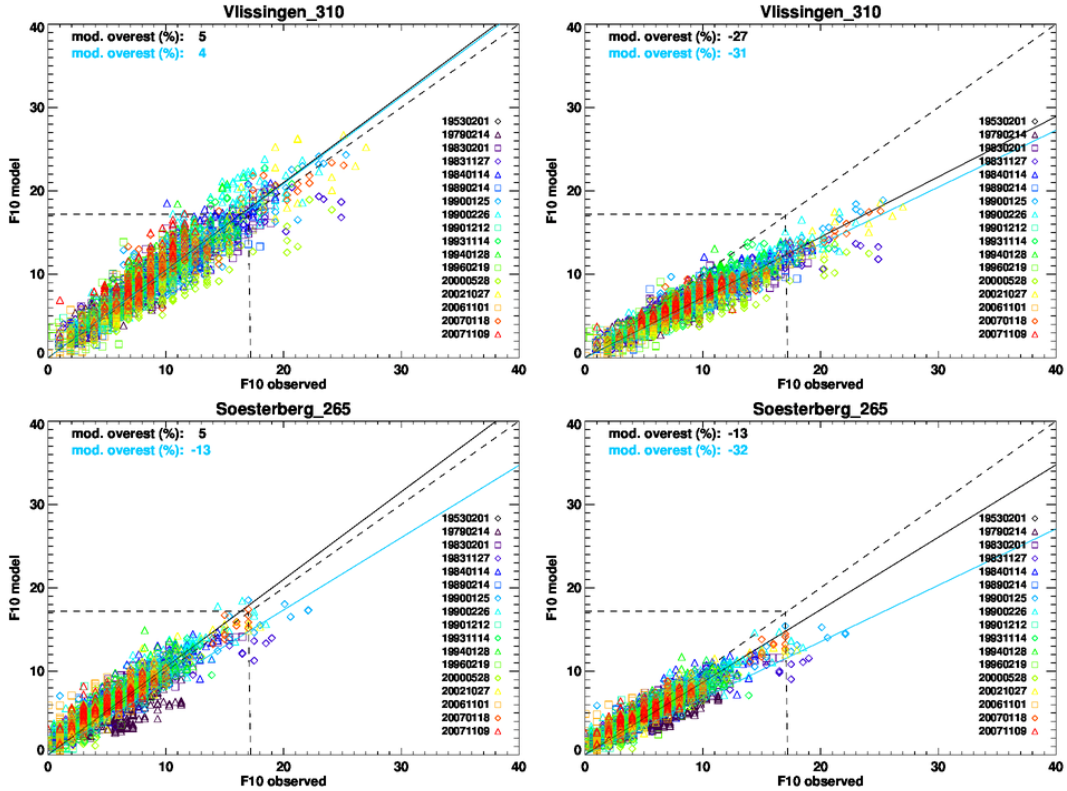

Figure 3.3. Modelled versus observed 10-m wind speed (m/s) for Vlissingen and Soesterberg. The left panels are based on the evaluation method described in the text, the right panels are based on the 'closest gridbox' approach. Black lines represent the best linear fit through all the data points, blue lines through data points which exceed the 8Bft threshold (indicated by the dashed lines) in either the model or the observations. Numbers indicate the modelled overestimation in %.

3.3 Temporal resolution of model output and observations

Besides hourly averaged observations, also the 10-minute averaged values just before the hour are available. The model state is available every hour. Here we discuss how the 'instantaneous' model values should be compared with the observations in order to obtain a fair comparison. Continuous 10-minute observations are available for some stations from 1995 onwards. Since 2003, 10-minute observations are archived for almost all stations (Wever and Groen, 2009).

Two different comparison methods were tested:

1. Hourly averaged observations (available for all storms) are compared with the average of two model wind fields: one valid at the start of the hour, the other at the end.
2. The 10-minute observations valid just before the hour (available for all storms) are compared with the model wind field valid at the hour.

Errors for method 1 were found consistently smaller than for method 2, which suggests that the model lacks small-scale variability in time and space or that the fluctuations at a 10-minute scale are not deterministic anymore (or a combination of both). The difference in rms error is typically 0.4 m/s. Based on these results, we adopt method 1 for the model evaluation. The method is illustrated in Figure 3.4. Note that the impact of time-averaging the model fields is negligible: when 'instantaneous' model fields are compared with hourly averaged wind speeds, bias and rms scores are virtually similar to the case in which the time-averaging is applied.

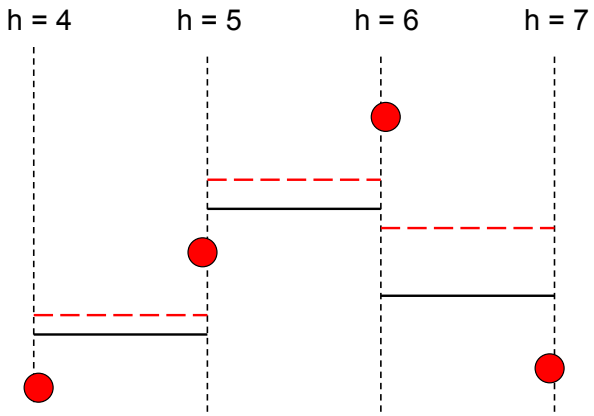

Figure 3.4. Schematic diagram of the method how the model is compared to the observations. Black solid lines: hourly averaged observations, red circles: model states at the hour, red dashes lines: average of two model states at the start and end of each hour.

To investigate the variability of the model and the observations in more detail, we performed a HARMONIE simulation with 10-minute output for 10-20 Jan 2007. For both the modelled and observed time series, we computed the sub hourly standard deviation of the 10-minute data. Typically, the variability in the observations is 50% higher than in the model.

Figure 3.5 shows time series of the wind speed and direction for K13 and Twenthe for 18 Jan 2007. Although the model shows some variability on time scales smaller than an hour, the variability in the observations is larger. In the afternoon and evening, the variability is strongly increased in both the observations and the model at both locations. This is due to the passage of lines of severe showers, which disturb the otherwise more homogeneous wind field. These results demonstrate that HARMONIE is able to represent not only the large-scale wind fields but also the impact of individual showers on the wind field, at least in a qualitative way.

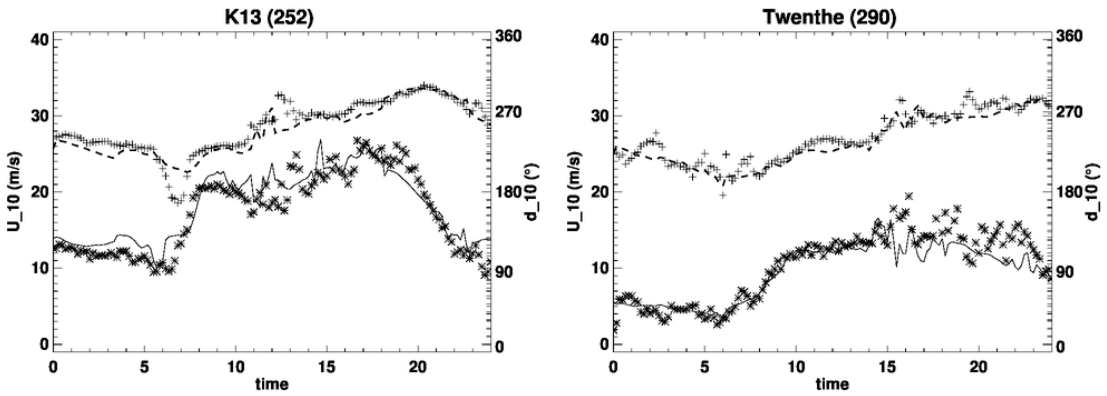

Figure 3.5. Time series of wind speed (m/s) and direction (°) for K13 and Twenthe. Solid lines indicate modelled wind speed, dashed lines modelled wind direction. Crosses indicate observed wind speed, plusses indicate observed wind direction.

3.4 Representation of atmospheric stability

3.4.1 Impact of atmospheric stability on surface wind

In specific atmospheric conditions, the 10-m wind speed over land is nearly as high as it is above the sea. Earlier reports, e.g. Caires *et al.* (2009), suggested that the stability of the lower atmosphere plays a role in this: when warmer air flows over a colder water surface, the wind speed above the water is likely to be reduced. Similar arguments, but in that case for Lake IJssel, are made by Bottema (2007).

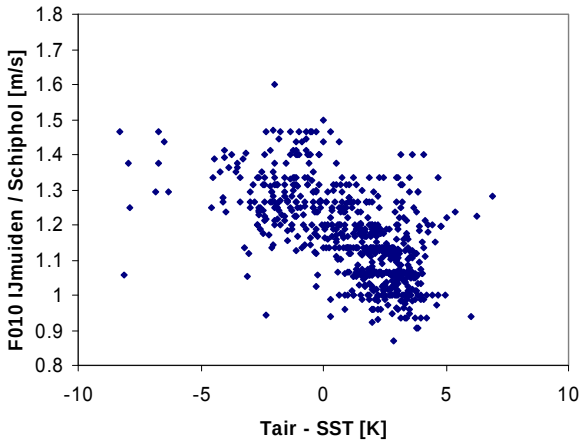

Figure 3.6. The 10-m wind speed ratio between IJmuiden and Schiphol as a function of the air-water temperature difference. Data from 1980-2010 have been used. Only data for which the wind speed at both locations exceeds 15 m/s and the wind direction is between 180° and 360° have been included. The air temperature denotes the average temperature of Hoek van Holland and De Kooy; the SST is the average of daily values observed at Lichteiland Goeree, Europlatform and Hoek van Holland.

Here we investigate this phenomenon in more detail by analyzing observations and by analyzing a model simulation of the 25 Jan 1990 storm with warmed sea surface temperature (SST) field. As demonstrated by Figure 3.6, observations show a clear decreasing trend in the 10-m wind speed ratio between IJmuiden and Schiphol for increasing air-water temperature differences. Apparently, atmospheric stability is able to modify the near-surface wind field even for wind speeds above 15 m/s.

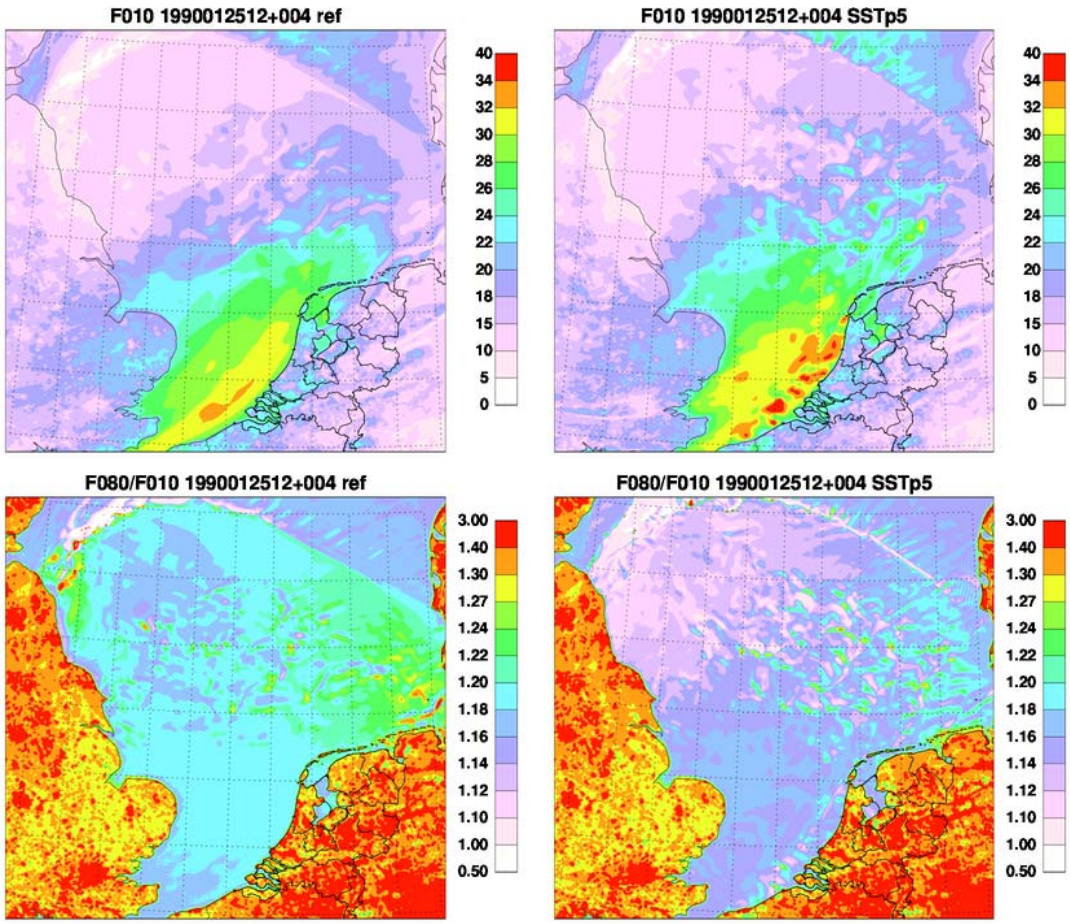

Figure 3.7. Simulated 10-m wind fields (m/s) (top panels) and wind speed ratios between 80 and 10 m height (bottom panels) for 25 Jan 1990, 16 UTC. Left: reference simulation. Right: simulation in which the SST is increased by 5 K.

Since the storm of 25 Jan 1990 was mentioned as a case in which the wind over land was relatively high compared to over sea, we did a sensitivity experiment with HARMONIE for this storm in which we enhanced the SST by 5K. By doing so, the sea becomes warmer than the air above and the stability of the lower atmosphere changes from stable to unstable. For the maximum of the storm, the 10-m wind fields are given in Figure 3.7. The increase in SST has a clear effect on the 10-m wind: over a large area it becomes several m/s higher than in the reference simulation with the SST unchanged. The increase is a direct result of the change in atmospheric stability, which enhances the vertical mixing over a much deeper

layer, thus mixing air with high momentum all the way down to the surface. The change in stability can also be inferred from the spatial structure of the wind field, which is more variable in the perturbed SST run than in the reference run. Again, this can be explained by the unstable conditions in which convective showers develop that modify the wind field leading to large temporal and spatial gradients (Portabella *et al.*, 2012).

It is interesting to consider the wind speed ratio between typical platform height (80 m) and the 10-m level as shown in the bottom panels of Figure 3.7. Does this information provide new insights in the applicability of the Benschop correction? Despite the significant impact on the 10-m wind speed, increasing the SST by 5 K has only a small influence on the wind speed ratio: the changes are in the order of 3-4%. These results are in line with the analysis of Section 2.1.3, which demonstrates that for high wind speeds the Benschop correction introduces only a small error in the 10-m wind speed.

These results are further illustrated by referring to Figure 3.8, which shows a cross-section of 10 m and 80 m wind speed across the North Sea. Not only the 10-m wind speed is increased by the higher SST, the 80 m wind speed increases nearly just as much. At heights of several hundreds of meters the situation is reversed: here the wind speed in the run with enhanced SST is reduced compared to the reference run. The large oscillation around 4°E visible in the cross section of the increased SST run is caused by the presence of vigorous convective showers that develop as a result of the unstable conditions.

Although for these high wind conditions the impact on vertical wind speed ratios in the lowest 100 m of the boundary layer may be limited, increasing the SST does have a significant impact on the water/land 10-wind speed ratio: while the wind speed over sea is increased, the wind speed over land is slightly reduced, which is related to the reduced wind at several 100 m of height. This implies that for stable conditions over sea (reference run) the near-surface water/land wind speed ratio is indeed relatively low.

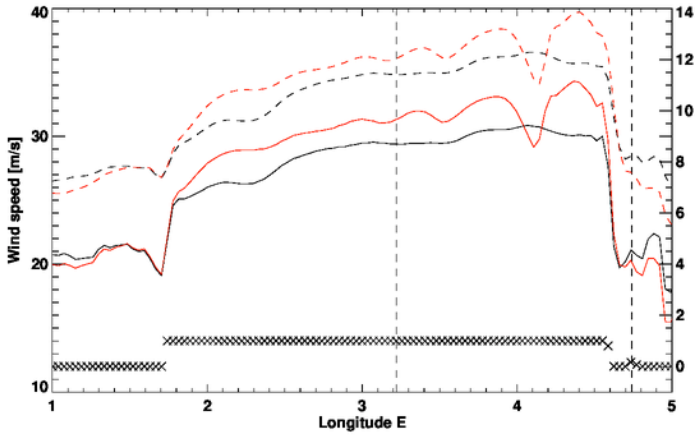

Figure 3.8. West-east cross sections of wind speed (m/s) over the North Sea at 52.5°N. Black lines indicate the reference simulation, red lines the simulation with increased SST. Solid lines indicate wind speed at 10 m height, dashed lines at 80 m height. Crosses indicate the HARMONIE sea fraction per grid point (right axis). Vertical dashed lines indicate the locations of K13 and Schiphol.

3.4.2 Comparison with tall mast observations

Here we compare stability characteristics of the model with observations from two measuring towers. The FINO1 tower is located over sea at approximately 50 km north of Schiermonnikoog. The tower is operated by the Bundesambt für Seeschifffahrt und Hydrographie (BSH). The Cabauw tower, operated by KNMI, is located over land in the centre of The Netherlands. For both locations, we use data from 2004-2009.

In recent years, many publications appeared in literature on the analysis of measuring towers at sea and the impact of stability on the wind profile (e.g. Lange *et al.*, 2004; Loriaux, 2011; Sathe *et al.*, 2011; Peña *et al.*, 2012). To quantify stability, various methods are available, most of them use Monin Obukhov Similarity Theory (MOST) in some way (Gratchev and Fairall, 1996). Differences between various methods are considerable, although they agree qualitatively. One of the main difficulties is that in order to quantify stability a vertical temperature difference is needed, which is often in the order of a few tenths of degrees (except for very stable conditions in which the difference is larger). Because this is in the same range as the accuracy of most observations, relative errors are large (Sathe *et al.*, 2011). Also, the wind in the upper parts of the masts may be subjected to inertial oscillations leading to low-level jets (e.g. Nunalee and Basu, 2013) and other non-stationary motions that invalidate the assumptions underlying MOST (e.g. Gryning *et al.*, 2007).

Here we present a qualitative analysis of the observed and modelled 80/40m wind speed ratio for the two locations as a function of the bulk Richardson number, Ri_b, in this case given by

$$Ri_b = \frac{g}{\theta}\frac{\Delta z \Delta \theta}{(\Delta U)^2} \ ,$$

where g is the acceleration due to gravity, z the height above the surface, θ the potential temperature and U the wind speed. The Δ refers to a vertical difference between 80 and 40 m.

Figure 3.9 shows the observed and modelled 80/40 m wind speed ratio for the two locations as a function Ri_b. For the model, data from all storm periods are used; for the observations all available data for the months December, January and February has been used. Focussing on the top panels, for which no threshold on the wind speed has been imposed, the observed wind speed ratio increases gradually until the Ri_b reaches its neutral value. Then, the ratio increases rapidly. The model responds to the change in stability in a similar way, but to a lesser degree. This is a known feature of the turbulent mixing scheme that HARMONIE applies (Muñoz-Esparza *et al.*, 2010). Since only data from the winter months are shown, unstable conditions are virtually absent at Cabauw. At FINO, unstable conditions do occur in winter as a result of the relatively warm water temperatures. At Cabauw, the wind speed ratios are larger because of the higher roughness length.

The lower panels show the same data, but only for data points with a 10-m wind speed over 17.2 m/s (at least 8 Bft). For these conditions, the data are clustered around the neutral value. The impact of stability on the 80/40 m wind speed ratio is much lower than when no

threshold on the wind speed is imposed. The model corresponds to the observations in a qualitative way. At FINO, observed ratios are higher than modelled. Observations indicate a roughness length of 0.02 m, which is a rather high value over sea. The number of data points at Cabauw is very small. Variations in stability and wind speed ratio are small.

In summary, from the above discussion we conclude that:

- the wind speed ratio between 80 and 40 m increases rapidly for stably stratified conditions both over land and over sea,
- the model reproduces this feature, but its response to stability is too weak,
- for wind speeds of 8 Bft and higher, conditions are close to neutral and the differences in the 80/40m wind ratio are limited.

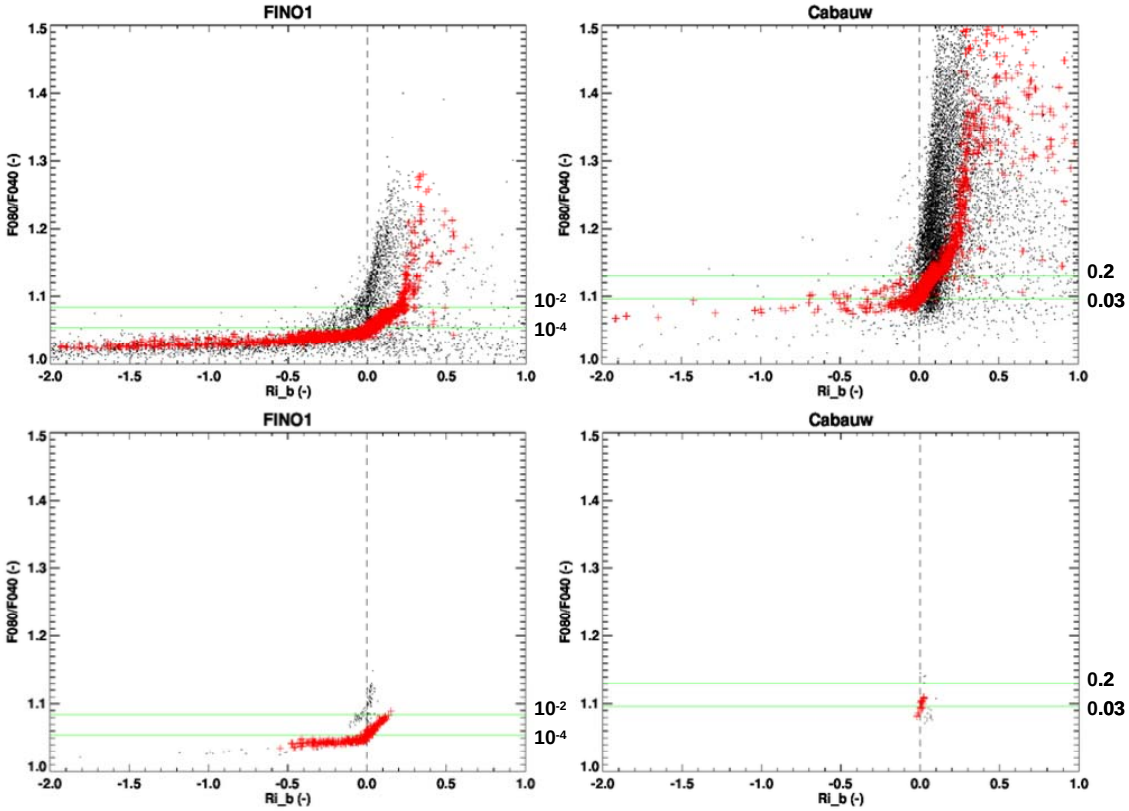

Figure 3.9. Observed and modelled 80/40 m wind speed ratios at the FINO (left) and at Cabauw (right) as a function of the bulk Richardson number. Top panels show data for all wind speeds, bottom panels for 10-m wind speeds exceeding 17.2 m/s (at least 8 Bft). Observations for December, January and February are indicated in black, model data for all hindcast periods in red. Horizontal green lines indicate 80/40 m wind speed ratios corresponding to specific roughness lengths (m) as indicated along the right axes.

4 Results

4.1 Evaluation of wind and pressure fields

4.1.1 Wind distributions

To investigate the general wind climatology of the model, empirical PDFs of the wind speed are considered. Figure 4.1 presents the PDF of the modelled and observed wind speed. It contains the hourly data for all 16 storms for all available stations. Summarized over all storms and all stations 117133 hours of data are included, which is the equivalent of 13 years. In general, the correspondence between model and observations is very good, indicating that the model has a realistic wind climate. The occurrence of extreme wind speeds is slightly too high in the model.

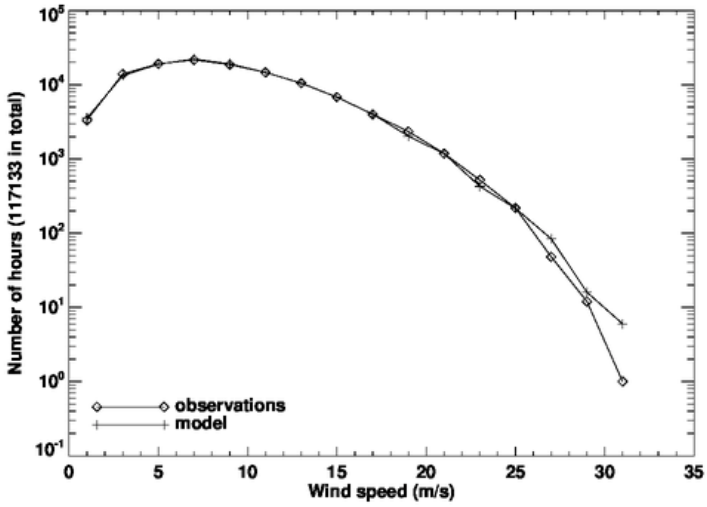

Figure 4.1. Distribution of modelled and observed 10-m wind speed (m/s) for all storms and all stations for bins of 2 m/s.

The occurrence of wind speeds exceeding consecutive Bft thresholds is summarized in Table 4.1. The results are split-up for stations over open water and over land (coastal stations are ignored). Absolute numbers between land and water are hard to compare because the number of stations is not the same, but it is clear that extreme wind speeds are much rarer over land than over water. Thus, the tail of the distribution shown in Figure 4.1 consists mostly of water cases, in particular for wind speeds over 10 Bft (24.5 m/s). Over water, the model overestimates the occurrence of extreme wind speeds, over land the number of extreme wind cases is underestimated. The differences between model and observations may seem larger than they actually are: small shifts in the wind speed distribution lead to significant changes in the number of exceedances of the respective Bft thresholds. This is especially true in the tail of the distribution. For example, over sea, the difference between model and observations corresponds to a 5 % overestimation of the modeled wind speed or, alternatively, as a positive bias of 0.5 m/s. The difference in number of occurrences of Bft 9 or higher over land corresponds to a negative bias of 1.5 m/s.

Table 4.1. Occurrence of observed and modelled wind speeds (number of hours) for consecutive Bft thresholds for stations located over open water and over land.

	Open water #obs | #mod	Land #obs | #mod
Bft 6 or higher	10962 | 11966	6588 | 6404
Bft 7 or higher	6014| 6480	2176 | 1747
Bft 8 or higher	2101 | 2391	578 | 386
Bft 9 or higher	574 | 680	118 | 28
Bft 10 or higher	77 | 153	9 | 0
Bft 11 or higher	5 | 8	0 |0
Bft 12 or higher	0 |0	0 |0

4.1.2 Temporal evolution

For each storm, Van den Brink *et al.* (2013) analyzed to what extent the wind speed maximum in the model simulation and the observation match. They concluded that over sea the storm maxima of HARMONIE show good correspondence with observations. Above land, they found a slight underestimation of the modelled maxima. No temporal trend in the quality of the simulations was found, indicating that the quality of the HARMONIE runs can be considered constant over the period considered.

Van den Brink *et al.* (2013) compared maximum attained wind speeds in the observations with maximum attained wind speeds in the HARMONIE simulations. In this way, differences in timing are not penalized. In this report, which aims for a more comprehensive verification of the model including temporal and spatial characteristics, we only compare modelled and observed values valid at the same time. For illustrating the difference between the two approaches, we compared for each storm and each station the maximum wind speed attained by the model (approach Van den Brink *et al.*, 2013) with the modelled wind speed at the time of maximum observed wind speed (approach present report). The difference between the two approaches amounts to 1.0 m/s on average: the former is 0.5 m/s lower than the observed storm maxima, the latter 1.5 m/s. These numbers are based on hourly averaged values for both the model and the observations.

4.1.2.1 Metrics of complete hindcast periods

Here we expand the analysis of Van den Brink *et al.* (2013) by considering not only the attained maxima in wind speed, but analyzing complete time series for each available station. This analysis will provide insight on the temporal evolution of the wind speed at each measurement location. Besides wind speed, also the wind direction and the mean sea level pressure will be analyzed.

Figure 4.2 presents the correlation coefficients between modelled and observed wind speeds for each station. Almost all stations show a correlation coefficient of over 0.9. Values over sea are close to 0.95, which is slightly but consistently higher than over land. The high

values indicate that, apart from possible biases, the model is able to capture the temporal evolution of the wind speed observations. The fact that differences between the stations are very small is encouraging.

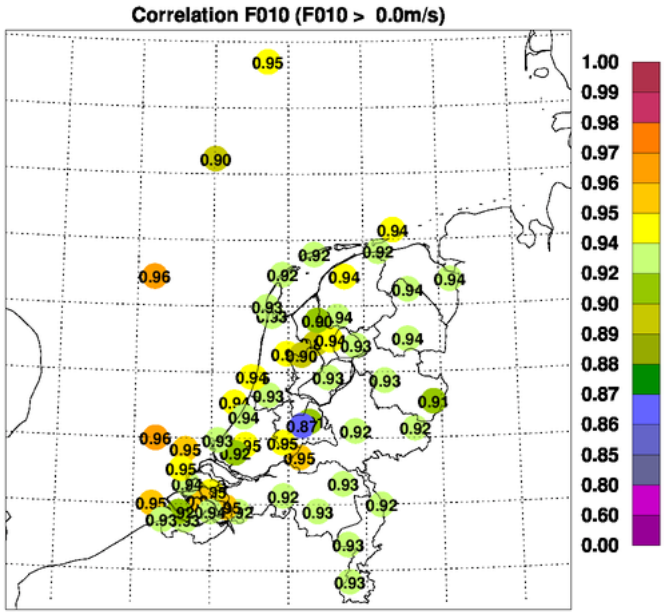

Figure 4.2. Correlation coefficients between observed and modelled 10-m wind speed for each station over all hindcast periods.

A more quantitative evaluation is provided by Figure 4.3. It presents bias and rms error scores for 1) all cases and for 2) only those cases in which the wind speed in either the model or the observation exceeds the 8 Bft threshold of 17.2 m/s. The results agree with the findings of Van den Brink *et al.* (2013). For both wind thresholds, a small positive bias of order 0.5 m/s is found over sea. Both over sea and over land rms errors are mostly between 1.5 and 2.0 m/s. Rms errors over land are slightly smaller than over sea, which is a result of the smaller average wind speeds. Over sea, the difference between the scores for the two wind thresholds is surprisingly small. Over land the situation is different: for winds of 8 Bft and higher negative biases appear for most of the stations and rms errors are increased. Differences between stations are larger than over sea. Despite the physical downscaling (see Section 3.2), the largest errors still occur for stations that are located in heterogeneous terrain. These findings are in line with other studies that also find that models have difficulties in reproducing extreme winds over land, see e.g. Lindenberg (2011). Although we are primarily interested in extreme wind speeds over water, model performance over land remains an intriguing topic for further research. Possible reasons may be related to vertical momentum transport in the model, the representation of internal boundary layers, or streamlining of the vegetation.

Figure 4.4 presents basic scores for wind direction. For both the total dataset and for wind speeds of 8 Bft and higher, the bias in wind direction is mostly within 5°, except for some coastal stations. The rms errors for winds of 8 Bft and higher is in the order of 10°, which is in

the same range as the accuracy of the observations. Differences between land and sea are small. Highest values are observed at coastal stations. Since the roughness transition along the coast induces a change in wind direction, at these stations an accurate prediction of wind direction is more challenging than over open water or inland. The increase of rms error in the wind direction when all wind speeds are taken into account is mostly due to wind speeds under 5 m/s. For these low wind speeds, the wind direction is much more sensitive to small small/random changes in the wind vector.

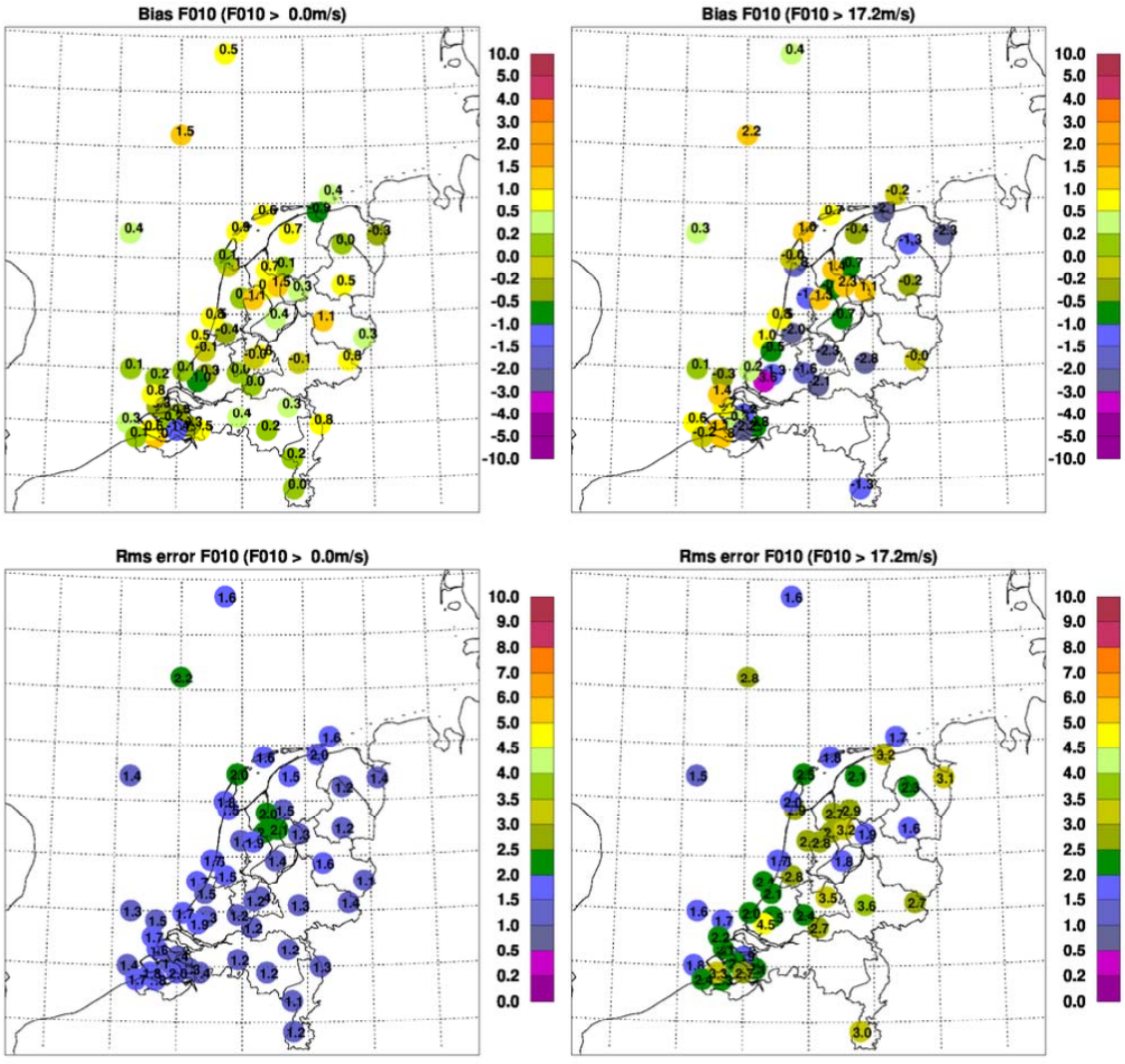

Figure 4.3. Bias (top) and rms error (bottom) scores per station for wind speed (in m/s). The left panels indicate values when no threshold on wind speed is imposed (at least 240 h data per station), the right panels indicate values for only those cases for which the wind speed in either the observations or the model exceeds 17.2 m/s (at least 12 h data per station).

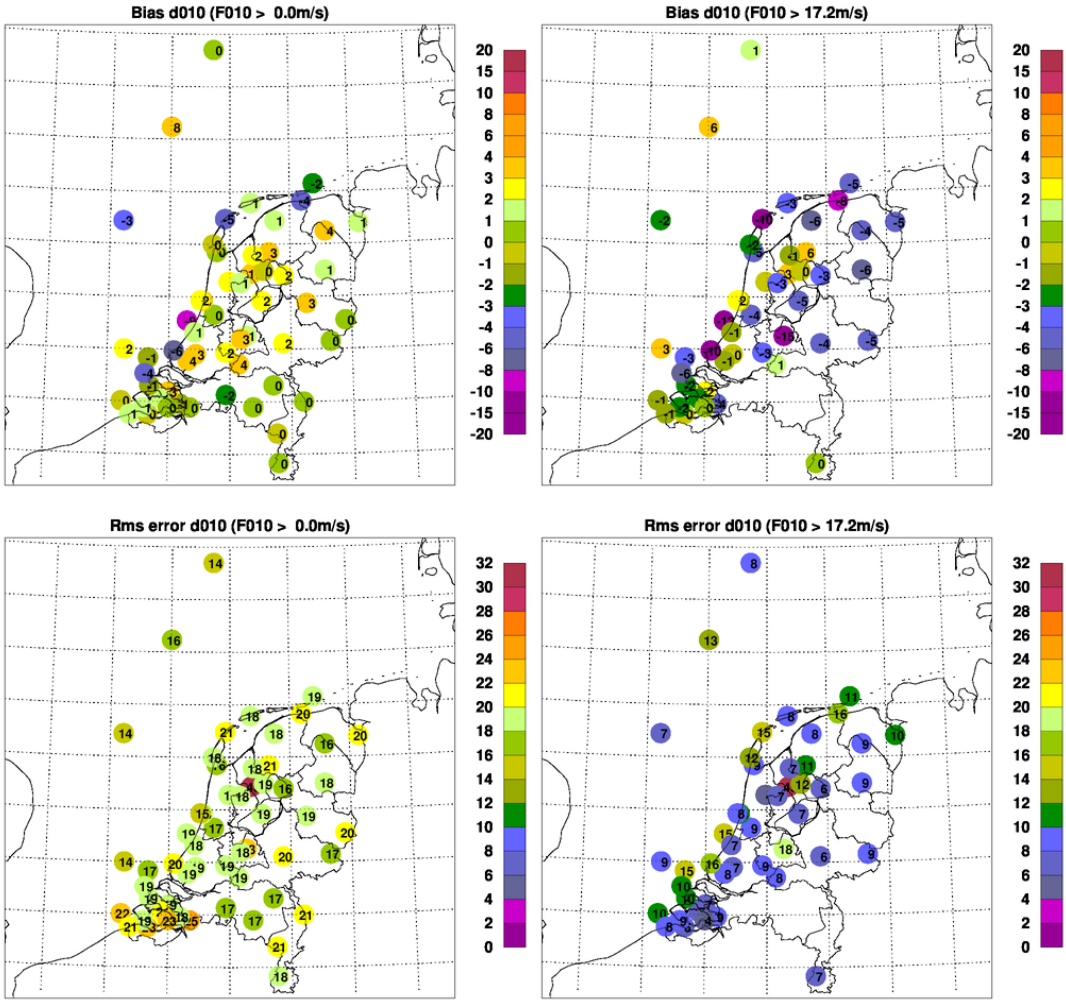

Figure 4.4. Bias (top) and rms error (bottom) scores per station for wind direction (in m/s). The left panels indicate values when no threshold on wind speed is imposed (at least 240 h data per station), the right panels indicate values for only those cases for which the wind speed in either the observations or the model exceeds 17.2 m/s (at least 12 h data per station).

The above results are presented in a different way in Figure 4.5, which shows density scatter plots of modelled versus observed wind speed and direction, split up in open-water stations and coast/land stations. For the wind direction plots only data with a wind speed of more than 5 m/s were selected. The model captures the variations in the observations well. The scores are consistent with the values in Figure 4.3.

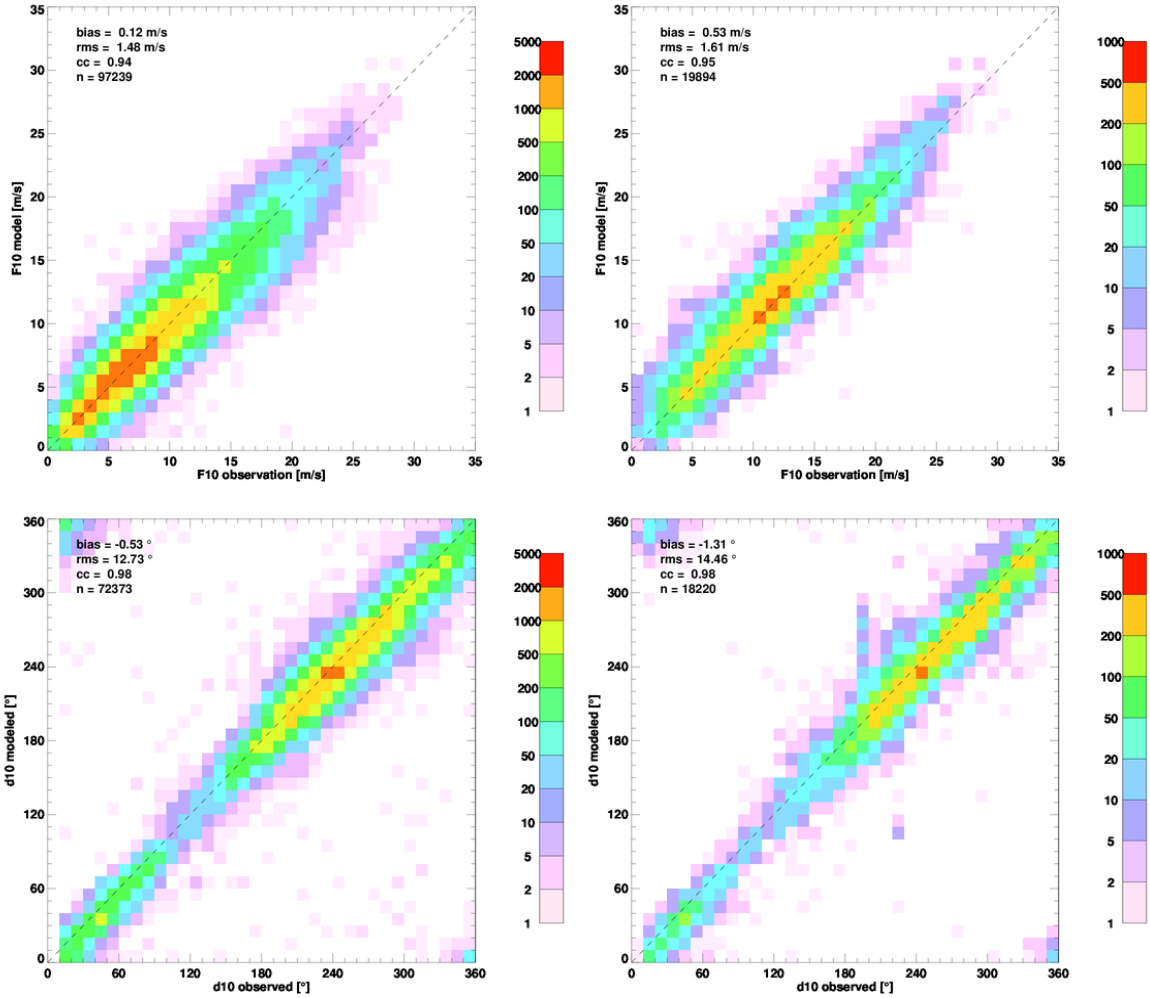

Figure 4.5. Density scatter plots of modelled versus observed 10-m wind speed (m/s) (top panels) and direction (°) (bottom panels) for coast/land stations (left panels) and open-water stations (right panels). For the wind direction panels only data points for which the wind speed exceeds 5 m/s are included. Colors indicate the number of occurrence for each bin.

4.1.2.2 Storm dependent scores

So far, average scores over all 16 storms have been presented. Next, we present scores for each storm individually to examine the variations in model performance between storms. Here, we focus on the evolution of the wind field associated with the main event of each hindcast period. Therefore, for each storm period we consider only the 24 h around the maximum observed wind speed at each station.

Figure 4.6 presents rms errors for pressure (left), wind speed (middle), and wind direction (right) for each of the 16 storms. No threshold on wind speed is imposed. We make a distinction between stations over sea, land, and along the coast. The quality of the modelled pressure evolution is rather equal for all storms. There is one notable exception: the storm of

27 Nov 1983. This relatively small, quickly developing system is not accurately captured by the model. In the southwest of The Netherlands large differences of up to 8 hPa between observed and modelled pressure values occur. This bad representation of the surface pressure is reflected in the wind speed scores for this storm. Generally, the quality of the wind speed is rather uniform among the storms with no trend in time (see also Van den Brink *et al.*, 2013). There is no clear distinction between different station locations. When only data over 8 Bft are taken into account the wind speed scores for the land stations deteriorate (not shown, see Figure 4.3).

The magnitude of the wind direction error appears to be related to the horizontal dimensions of the storm: for small storms with the centre of low pressure close to The Netherlands the variation in wind direction in time is large. Therefore, it is not surprising that the storms of 27 Nov 1983, 14 Nov 1993, and 28 May 2000 show the highest errors.

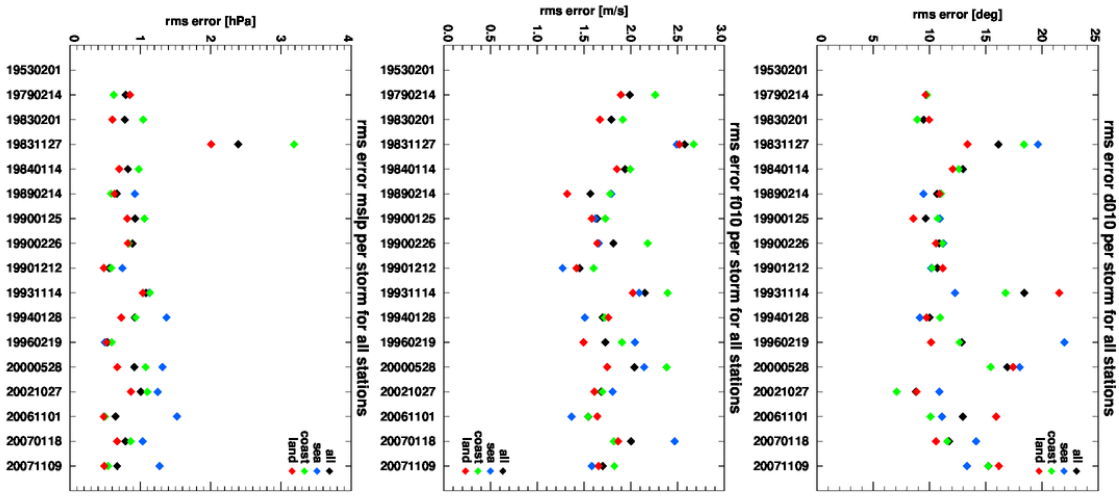

Figure 4.6. Station-averaged rms-error for pressure (left), wind speed (middle), and wind direction (right) for each of the 16 storms. For each station, only data within 12 hours before and 12 hours after the maximum observed wind speed are included. Colors indicate a subset of the stations: sea (blue), coast (green), land (red) and overall (black).

4.1.2.3 Modelled and observed rate of change of wind speed and pressure

For the stations K13, Schiphol, and Europlatform, we analyzed the rate of change in the hourly averaged 10-m wind speed and mean sea level pressure from one hour to the next (Figure 4.7). The results are based on the 24 h around the storm peaks. Observed hour-to-hour variations in wind speed can rise to 10 m/s. Maximum increase rates are larger than maximum decrease rates. The model reproduces the observations reasonably well. The extreme rates of change are underestimated. This underestimation is larger over land than over sea. Since these results are based on a direct comparison of modelled and observed time series, small mismatches in timing will increase the scatter.

The model captures the mean sea level pressure changes better than the rates of change in the wind speed. Differences between the stations are small.

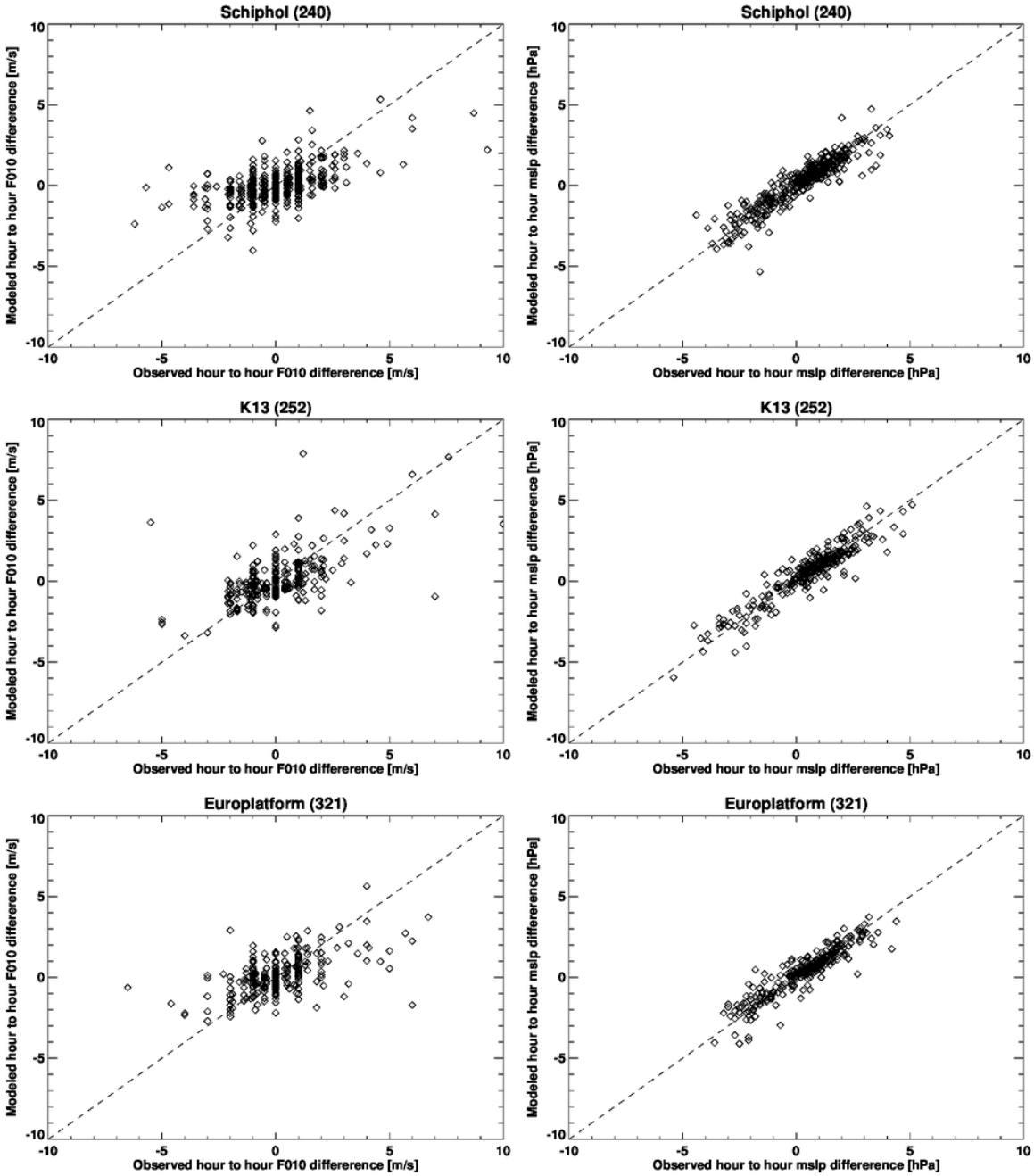

Figure 4.7. Modelled and observed hour-to-hour variations in wind speed (m/s) (left panels) and surface pressure (hPa) (right panels) for Schiphol, K13 and Europlatform.

4.1.3 Spatial characteristics

4.1.3.1 Metrics of spatial correspondence

Here we evaluate to what extent the spatial patterns in the modelled wind fields meet the patterns visible in the station observations. For each wind field, we take the available observations valid at the same moment in time as a reference. The scatter plots of Figure 4.8 show two cases with contrasting model quality. The right panel shows good correspondence for 8 Nov 2007 (10UTC), the left panel shows bad correspondence for 27 Nov 1983 (4UTC). Simple metrics quantify the difference in spatial correspondence between these two cases: for the 1983 case the correlation coefficient, rms error and bias are 0.85, 5.0 m/s and -4.3 m/s. For the 2007 case, these numbers are 0.95, 0.96 m/s, and 0.52 m/s, respectively.

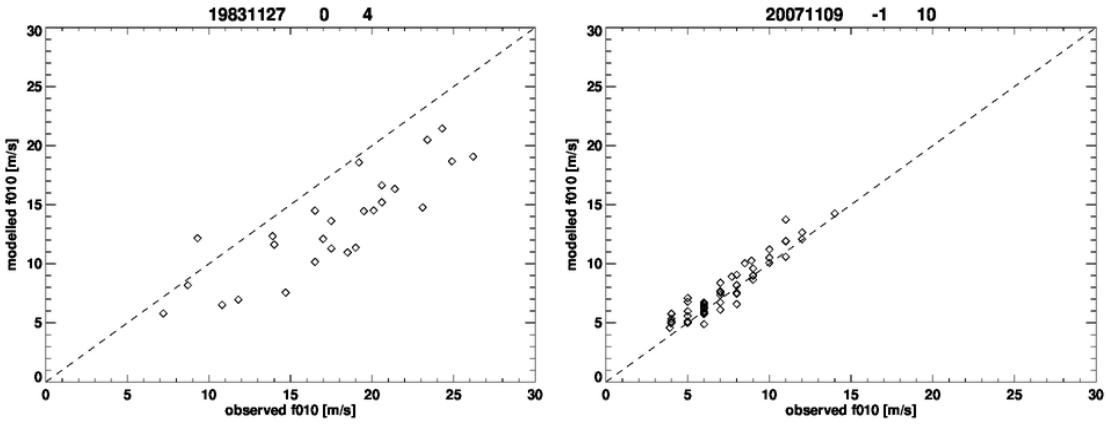

Figure 4.8. Modelled versus observed wind speed (m/s). Example of good spatial correspondence (right) and bad spatial correspondence (left).

Scores were calculated for all available wind speed fields (based on model simulated from 1 day before to one day after the main event). Pdfs are shown in Figure 4.9. Spatial correlation between observed and modelled fields is on average 0.87, indicating that in principle the model reproduces the observed spatial patterns.

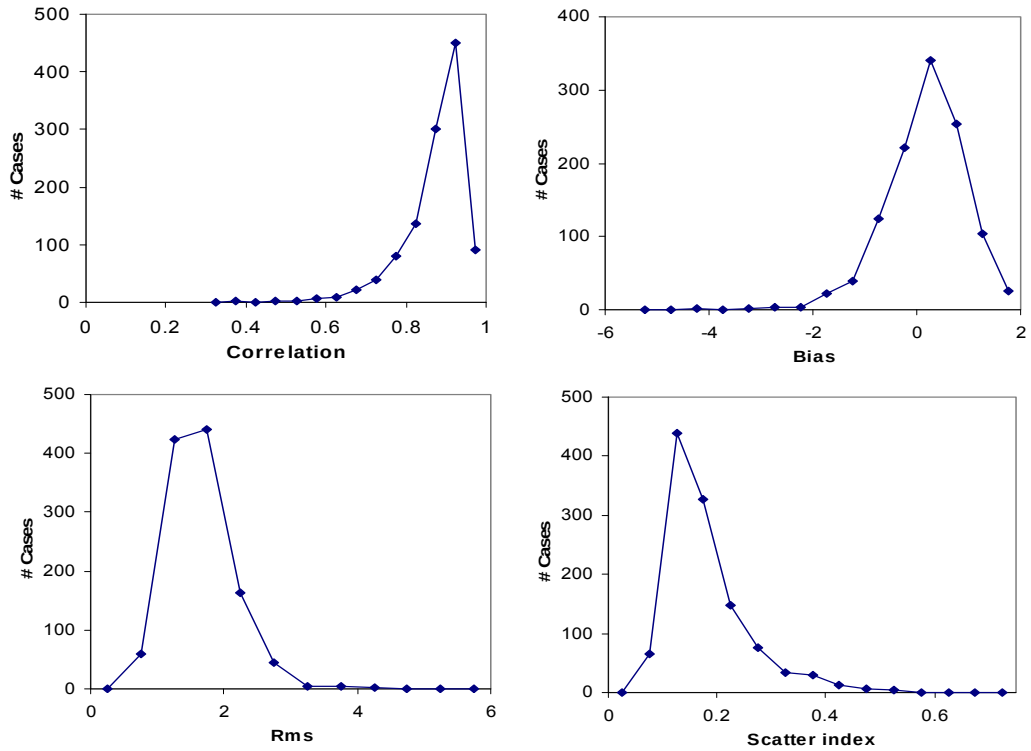

Figure 4.9. Pdf of spatial metrics of modelled and observed wind speed fields.

4.1.3.2 Spatial gradients in model and observations

To get a better feeling for the correspondence between modelled and observed spatial gradients, we consider wind speed and pressure gradients for a few selected stations.

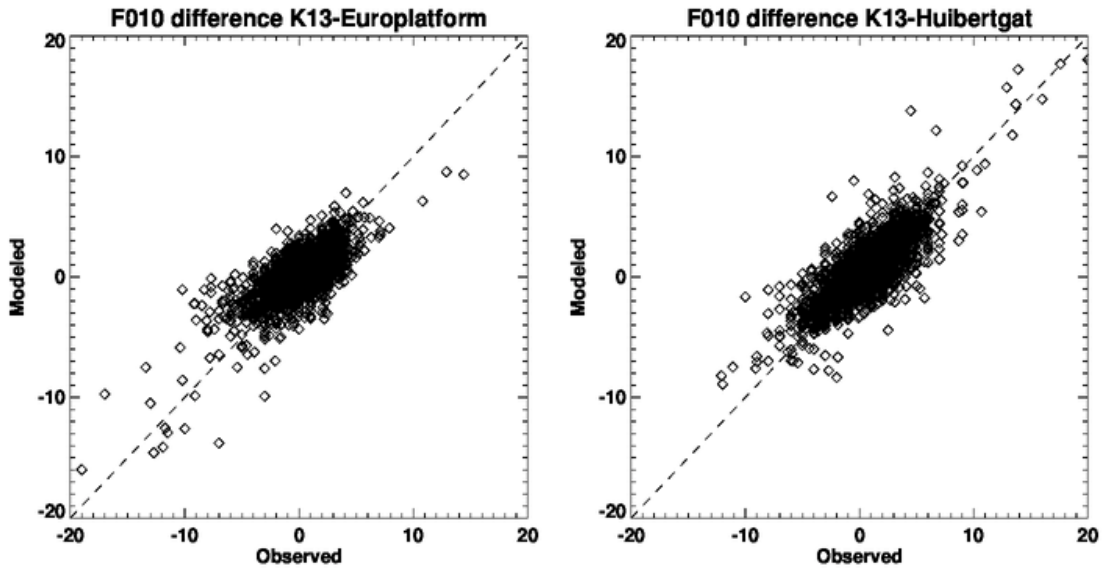

Figure 4.10. Modelled versus observed difference in 10-m wind speed (m/s) between K13 and Europlatform (left) and K13 and Huibertgat (right).

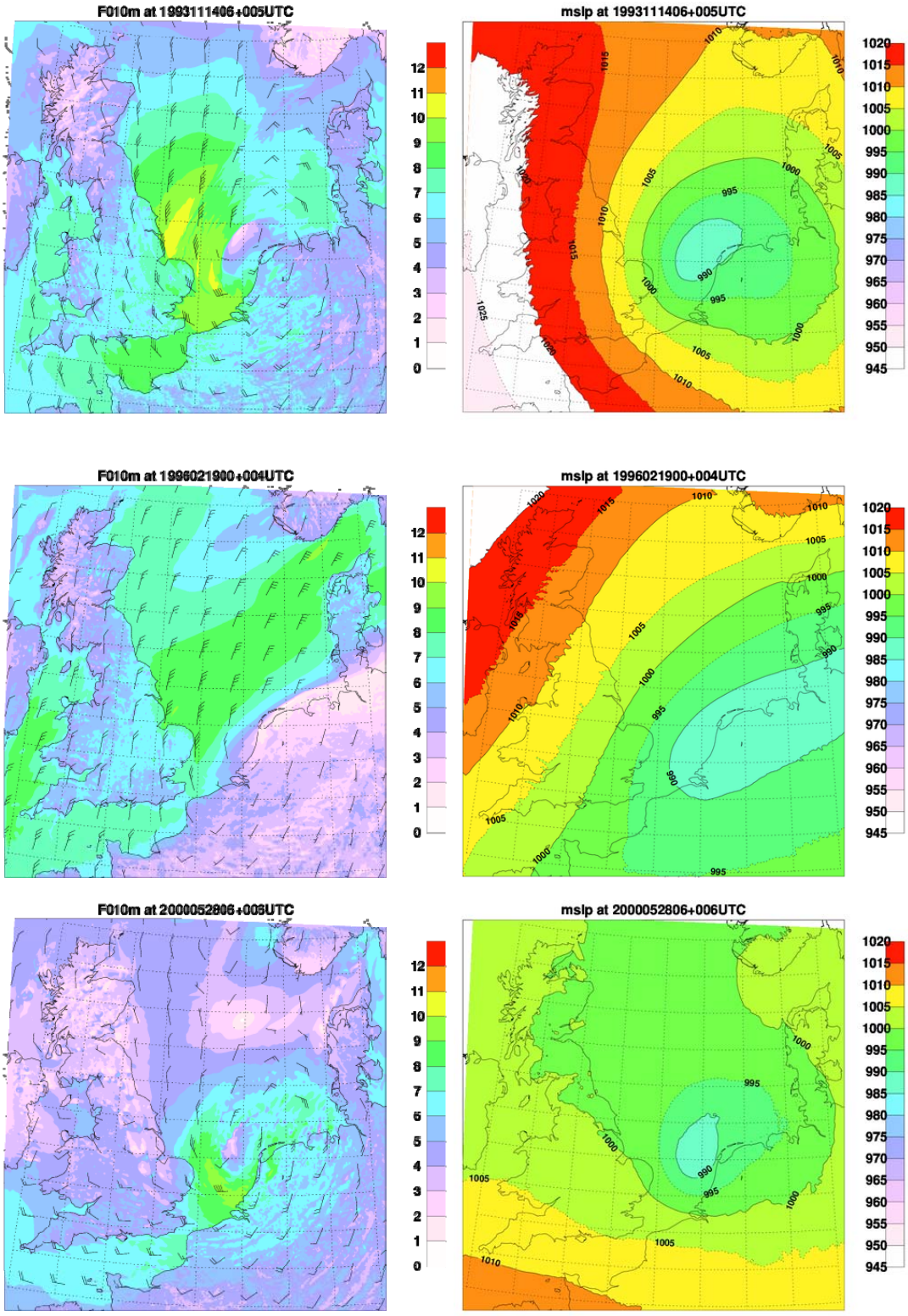

Figure 4.11. Examples of situations with large wind speed gradients near The Netherlands. The left panels show the wind speed (Bft). The corresponding pressure fields (hPa) are given in the right panels. Top: 14 Feb 1993, middle: 19 Feb 1996, bottom: 28 May 2000.

For wind speed, Figure 4.10 presents differences between K13 and Europlatform (north-south) and between K13 and Huibertgat (west-east). For most of the storms, differences between the stations remain below 5 m/s. However, for several storms the spatial gradients become large. The three largest observed differences between K13 and Europlatform are observed at 19 Feb 1996. Also the corresponding model differences are the largest in the record, although the magnitude is too low. Also between K13 and Huibertgat a large wind gradient is present for this storm. Only the storm of 14 Nov 1993 shows larger values. Both in the model and in the observations, large negative differences between K13 and the two other stations are registered for 28 May 2000 and 14 Nov 1993. The enhanced scatter for the difference between K13 and Europlatform is mainly caused by a difference in timing of about 2 h.

Large spatial gradients in wind speed occur in the vicinity of the low pressure centre. For the three storms mentioned in the previous paragraph, this is illustrated in Figure 4.11 by the modelled wind and pressure fields. We conclude that the HARMONIE produces realistic spatial gradients. Quantitative correspondence on case-basis depends on subtle differences in timing and position.

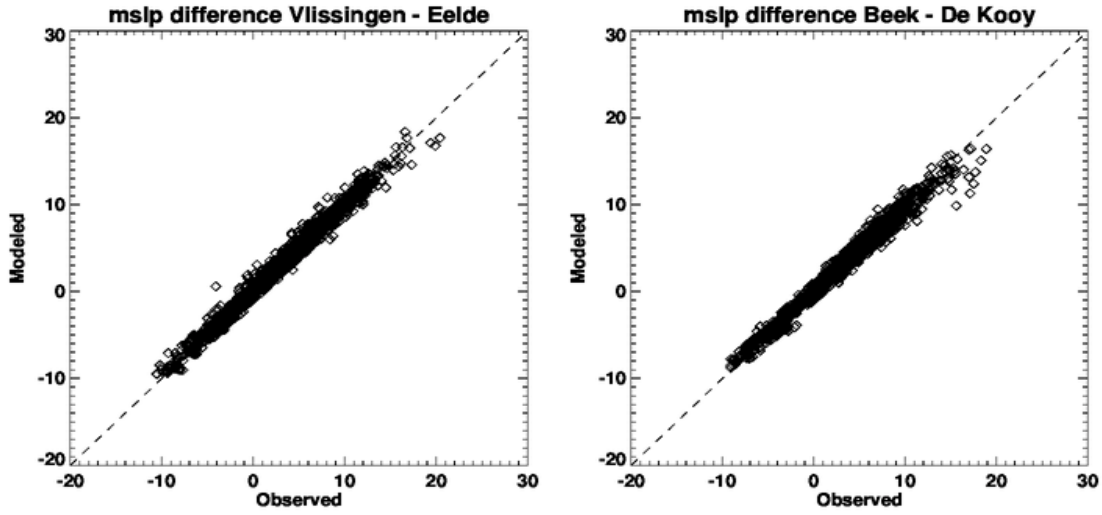

Figure 4.12. Modelled versus observed difference in surface pressure (hPa) between Vlissingen and Eelde (left) and Beek and De Kooy (right).

Figure 4.12 shows observed pressure differences between Vlissingen and Eelde (southwest-northeast) (left) and Beek and De Kooy (southeast-northwest) (right). Pressure gradients are important since they determine the geostrophic wind. Analysis of the gradients may confirm or deny whether systematic errors in surface pressure representation play a role in and under/overestimation of the wind speed.

For most cases, the modelled and observed pressure differences closely agree; no systematic bias exists. In 87% of the cases, the absolute discrepancy between modelled and observed difference is less than 1 hPa. No difference in model performance for westerly

(positive differences) and easterly (negative differences) winds is found. Largest discrepancies between model and observations are found for the storm of 27 Nov 1983, with the model underestimating the pressure gradient with almost 6 hPa. Pressure differences up to 20 hPa are observed over The Netherlands. Such large pressure gradients occur both for storms with a small and for storms with a large spatial extension. In case of the former, the pressure centre is often located close to the Netherlands (27 Nov 1983, 28 May 2000), in case of the latter the pressure centre is often located between Scotland and Denmark (25 Jan 1990, 27 Oct 2002) (see Figure 4.13 for two examples).

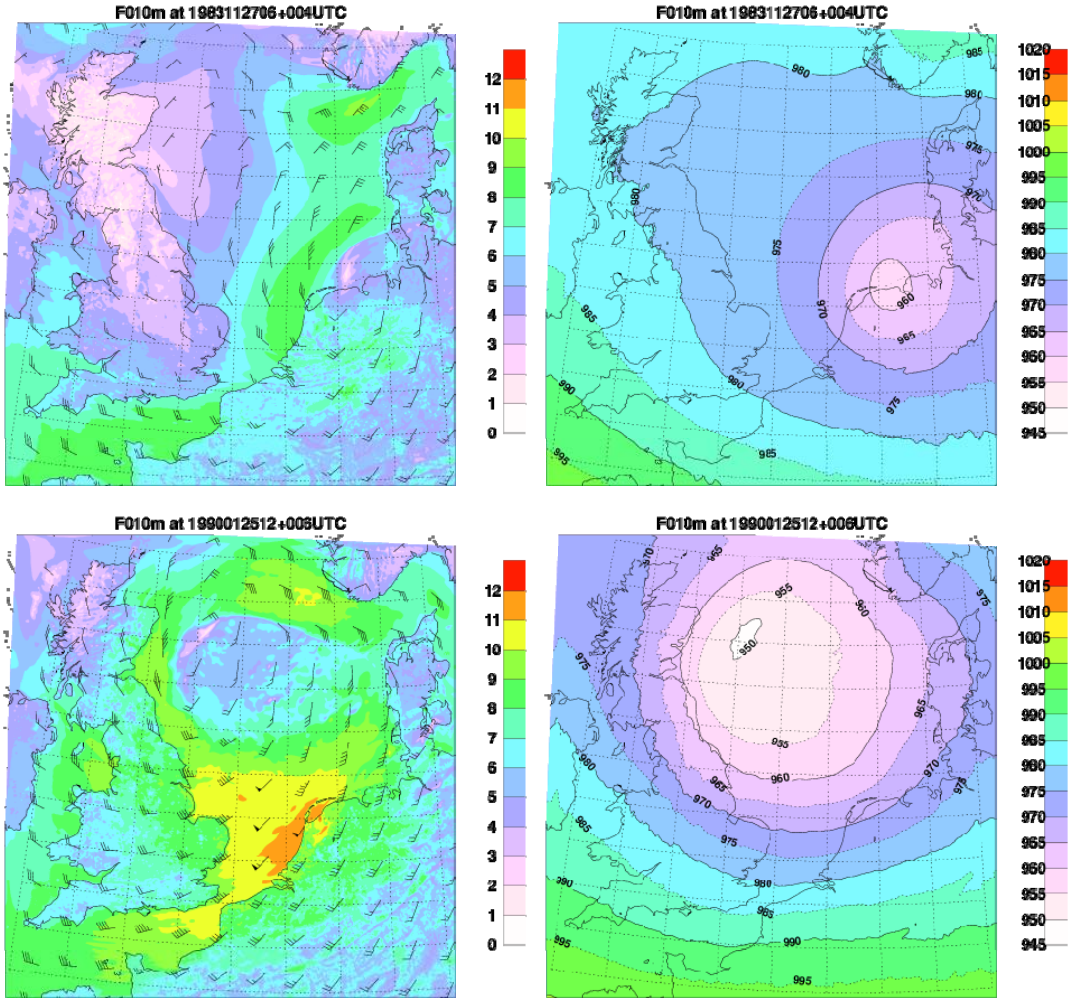

Figure 4.13. Examples of situations with large pressure gradients over The Netherlands. The left panels show the wind speed (Bft). The corresponding pressure fields (hPa) are given in the right panels. Top: 27 Nov 1983, bottom: 25 Jan 1990.

4.1.4 Comparison with scatterometer winds

Contrary to station observations, scatterometer data provide extensive spatial coverage over sea. Figure 4.14 gives an example of a scatterometer wind field. The corresponding HARMONIE wind field is given for comparison. The spatial structures are similar in both panels. In both the scatterometer image and the HARMONIE field peak wind reaches 8 Bft northwest of the Wadden islands. For each pair of collocated scatterometer-HARMONIE wind fields the spatial correlation has been calculated. A pdf of the correlations is provided in Figure 4.15. The distribution peaks at values between 0.85 and 0.90. The results indicate high spatial correspondence between the observed and modelled wind fields.

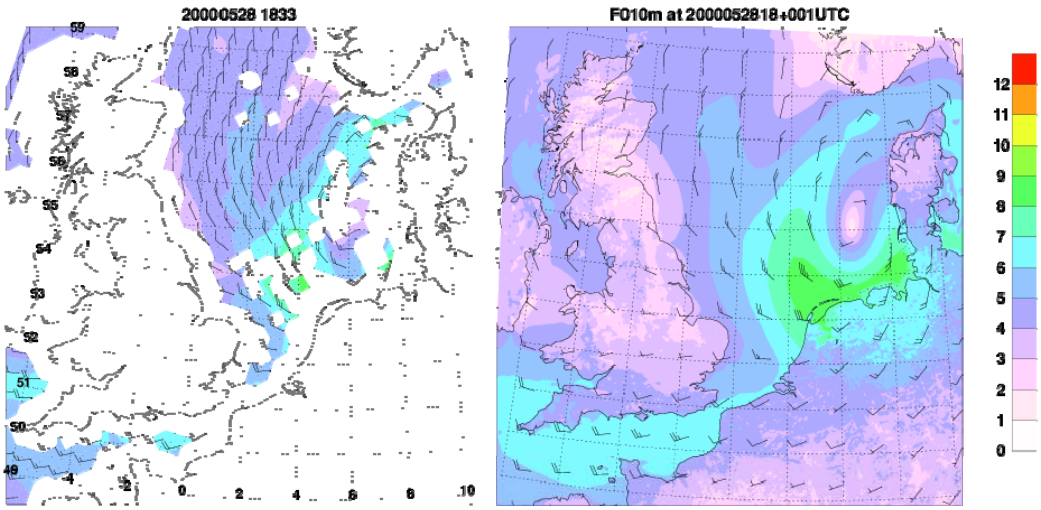

Figure 4.14. Example of a scatterometer image (left) and the corresponding HARMONIE wind field (right). Wind speeds are in Bft.

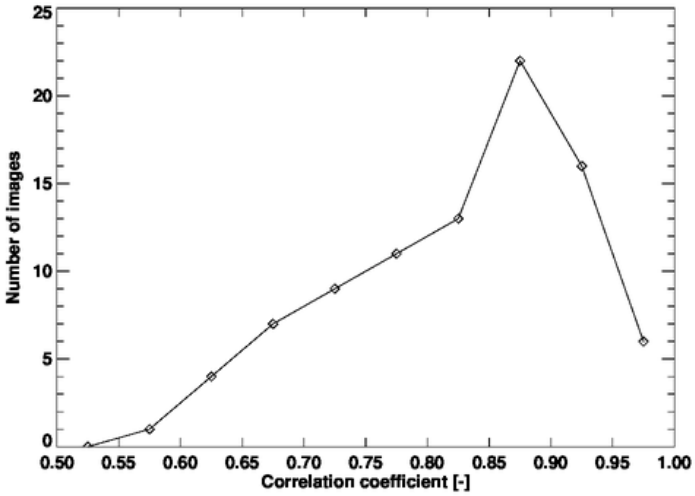

Figure 4.15. Pdf of spatial correlations of all collocated scatterometer images and HARMONIE wind fields (only images with more than 50 matches are included).

Figure 4.16 shows density plots for wind speed and direction for all collocated scatterometer-HARMONIE data points (34789 in total). The bias / rms error in the wind speed amounts to 0.57 / 1.65 m/s. In the wind direction the bias / rms error amounts to 0.87 / 15.9°. These numbers are close to numbers obtained from the comparison with station data (Section 4.1.2.1). For the wind direction comparison only observations over 5 m/s are taken into account.

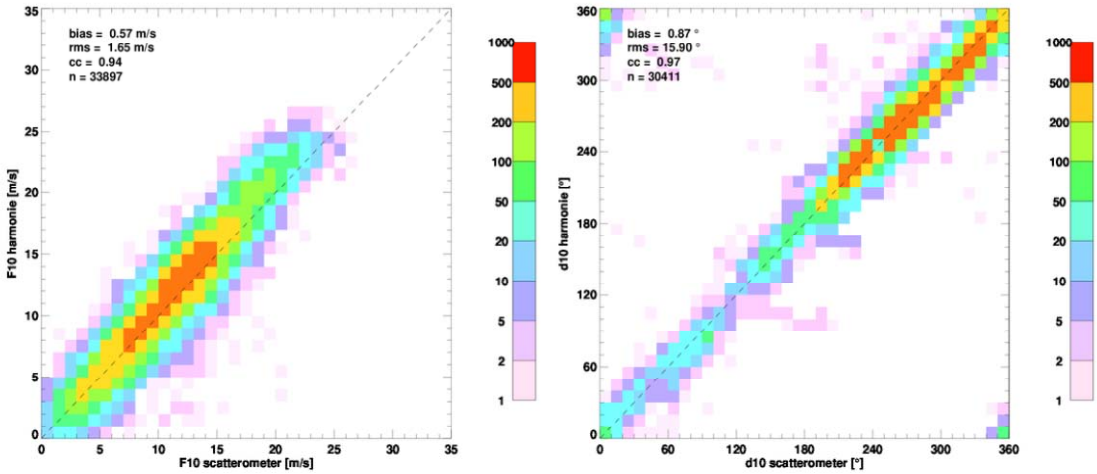

Figure 4.16. Scatter density plots of HARMONIE 10-m wind vs scatterometer winds. Left: wind speed (m/s), right: wind direction (°).

4.2 Wind patterns over Lake IJssel

In this Section, we focus on the representation of the wind field over Lake IJssel. The results can be interpreted as a case study on how HARMONIE represents land-water transitions. RWS station observations will be used as a reference.

Figure 4.17 shows average wind speed fields for the Lake IJssel area over all available HARMONIE forecasts of the 16 storms. The left panel shows the average wind field for westerly winds (wind direction at FL26 and FL2 between 240 and 300°), the right panel shows the average wind field for easterly winds (wind direction at FL26 and FL2 between 60 and 120°). As the air starts flowing over the water, a sudden increase in wind speed is visible. When the fetch over water becomes longer, the wind speeds still increases but at a slower rate. This initial fast and later more gradual adjustment agrees with the internal boundary layer model by Kudryavtsev *et al.* (2000). Halfway the lake the lines of equal wind speed still follow the shape of the coastlines. Similar patterns are observed in other water areas. For example, in the Wadden Sea a clear wind shadow is visible at the lee side of the islands (not shown).

Note that the presented wind speeds are not a wind climatology over Lake IJssel. Due to the selection of 16 storm periods they are biased to high wind speeds. Here we focus on the spatial patterns.

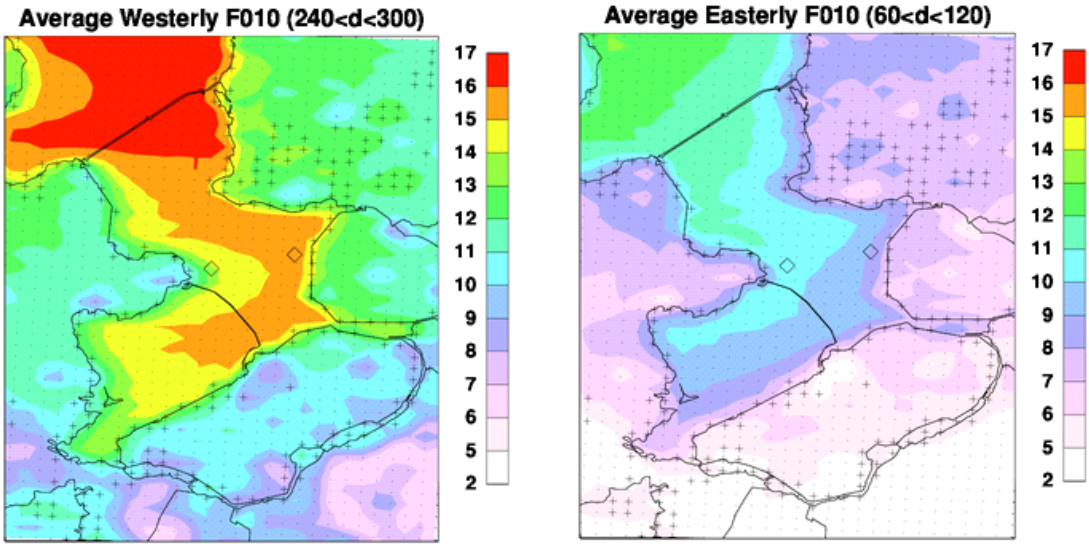

Figure 4.17. Average modelled wind speed over Lake IJssel for westerly (left) and easterly (right) winds (in m/s). The diamonds indicate the station locations (FL26 = left; FL2 = right). Dots indicate the HARMONIE grid, plusses indicate mixed land-water grid points.

Figure 4.18 shows west-east cross-sections of the 10-m wind speed normalized by the wind speed observed at FL2 for westerly and easterly winds. For both cases, the modelled FL26/FL2 ratio is close to the observed values, which are indicated by the asterisks. The transition from land to water is much more gradual than vice versa.

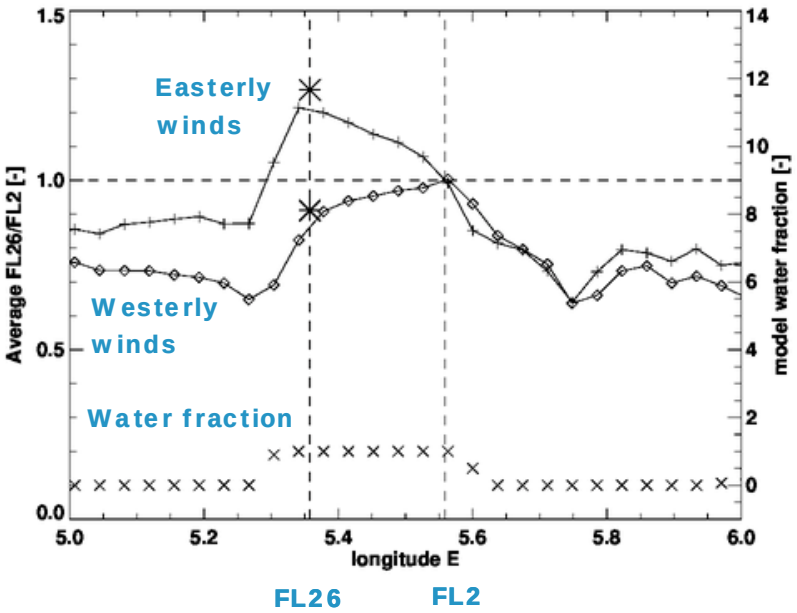

Figure 4.18. Cross section of westerly (diamonds) and easterly (plusses) 10-m wind speed along Lake IJssel, normalized with the wind speed at FL2. The asterisks indicate observed values. Crosses indicate the HARMONIE water fraction per grid point (right axis).

Following Bottema (2007), also the FL26/FL2 ratio versus the wind speed has been examined. Figure 4.19 shows the observed climatology shown by Bottema (2007; Figure 4.7) (left) and HARMONIE values for the 17 hindcast periods. The absence of low wind speeds in the model demonstrates that the subset of 17 storm periods is not representative for the Lake IJssel wind climatology. Still interesting similarities exist. In both the observations and the model the scatter decreases for higher wind speeds. This is related to the decreasing impact of atmospheric stability for higher wind speeds. Also the weakly increasing trend in the observations is also present in the model. Modelled absolute values are slightly lower than observed. This is partly due to the 'nearest gridpoint' approach for open-water stations: FL26 is just between two HARMONIE gridpoints. When the eastward gridpoint would have been selected, modelled values would equal the observed ones, as can be inferred from the cross-section in Figure 4.18.

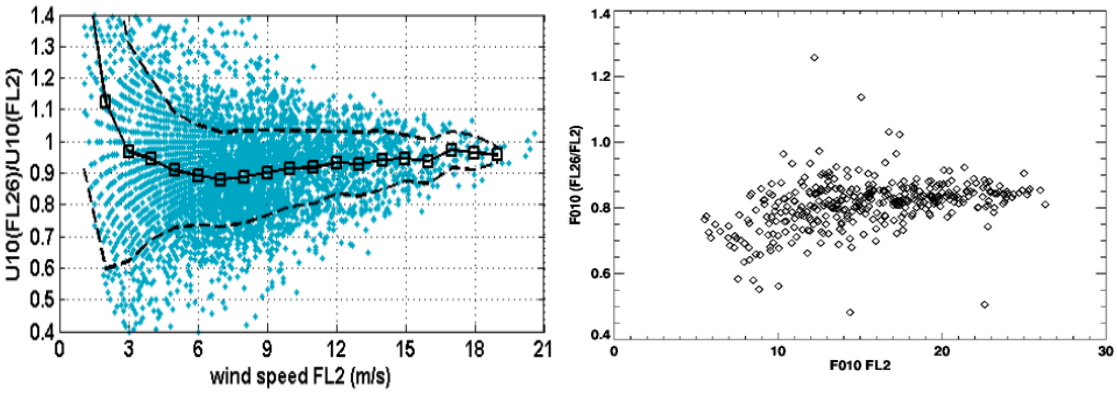

Figure 4.19. Wind speed ratio FL26/FL2 as a function of the wind speed at FL2. Left: data from Bottema (2007). Right: data from HARMONIE. Note that the x-axes range is different for the two panels.

Bottema (2007) demonstrates that part of the scatter present in Figure 4.19 can be attributed to atmospheric stability effects. The left panel of Figure 4.20 is a reprint of Bottema (2007, Figure 4.8), showing that the wind ratio FL26/FL2 increases with increasing temperature difference between air and water for different wind speed classes. The right panel shows the same plot for the HARMONIE simulations. HARMONIE water temperatures are taken from the ERA-Interim dataset. Water temperatures in ERA-Interim are based on various global datasets that include both satellite and in-situ observations (Dee *et al.*, 2011). The similarities between model and observations are striking. For example, in both panels the sensitivity of the wind speed ratio to air-water temperature difference decreases with increasing wind speed. As noted by Bottema (2007) this is because the stability is not only a function of the vertical temperature difference, but also of the wind speed itself.

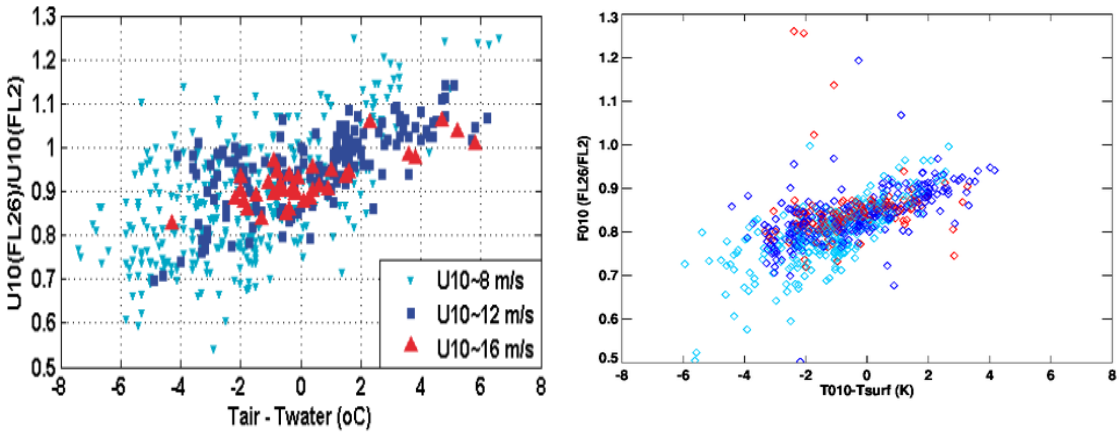

Figure 4.20. The effect of increasing air-water temperature difference on the wind speed ratio FL26/FL2. Left: observed values (adopted from Bottema (2007)). Right: HARMONIE data.

The results in this Section indicate that HARMONIE is not only able to capture the wind patterns at Lake IJssel induced by land-water transitions, but is also able to incorporate the impact of atmospheric stability on the wind field.

4.3 Surface stress

This report focuses on the representation of the near-surface wind field. However, in the end it is the surface stress that is needed to drive waves and the evolution of the surge. Stress values are tightly coupled to the wind speed by the drag relation, which is given by

$$\tau = \rho C_d U^2,$$

where τ is the surface stress, ρ the density of the air, C_d the drag coefficient and U the wind speed. The drag coefficient itself also depends on the wind speed as shown in Van den Brink et al. (2013, their Figure 2.1). For convenience, this figure is reproduced here (Figure 4.21). The spread among the data points is caused by differences in atmospheric stability. As can be seen, the impact of stability on the drag relation is relatively small.

Unfortunately, a direct verification of the modelled surface stress fields against observations is not yet feasible. Instead, we compare wind and stress fields. As an example, Figure 4.22 shows the modelled surface stress and 10-m wind fields for 27 October 2002, 15 UTC. Over sea, the surface stress is largest in areas with the highest wind speed. Over land the opposite is true. Here the highest stress values are reached in areas with the lowest wind speed, e.g. over the forest of the Veluwe and the agglomerations of Amsterdam and Rotterdam.

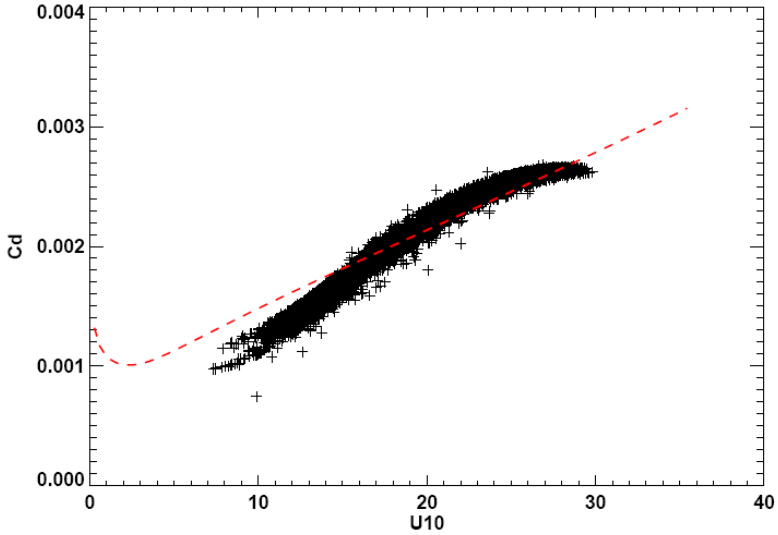

Figure 4.21. The ECUME drag relation as diagnosed from the stress and 10-m wind fields (symbols) and a Charnock relation with α = 0.020 (dashed line).

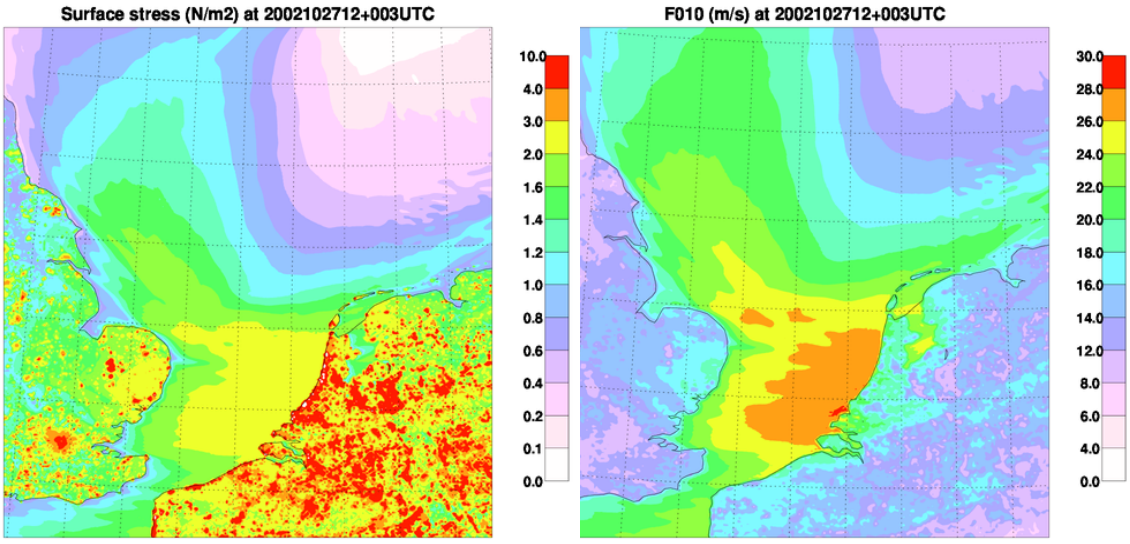

Figure 4.22. Surface stress (N/m^2) (left) and 10-m wind speed (m/s) (right) for 27 Oct 2002, 15 UTC.

4.4 Comparison between HARMONIE and ERA-Interim

The HARMONIE simulations (grid spacing of 2.5 km) are driven by ERA-Interim reanalyses (grid spacing of approximately 80 km). In previous sections, the quality of HARMONIE wind fields has been assessed. Here we discuss the differences and the added value of the high-resolution HARMONIE fields over the ERA-Interim fields.

Figure 4.23 presents HARMONIE and ERA-Interim wind fields for 25 Jan 1990, 18 UTC. It demonstrates four characteristic differences between the two model sources:

1. The large-scale spatial structures in the wind field are identical for both models. For example, the shape and location of the area with winds lower than 16 m/s in the Northern part of the North Sea. Also the wind direction is very similar among the two fields.
2. HARMONIE resolves much more small-scale structures as ERA-Interim. For example, these can result from outflow around convective showers. Over land, the detailed roughness map is clearly visible in the HARMONIE wind field (towns, forests).
3. In HARMONIE the coastlines are sharply defined, in ERA-Interim they appear as a gradual transition from water to land. Water bodies like Lake IJssel and the Waddensea are accurately resolved in HARMONIE. In ERA-Interim these are absent.
4. HARMONIE winds are generally higher than ERA-Interim winds, especially over sea. This is likely caused by a combination of difference in resolution and in applied drag formulation.

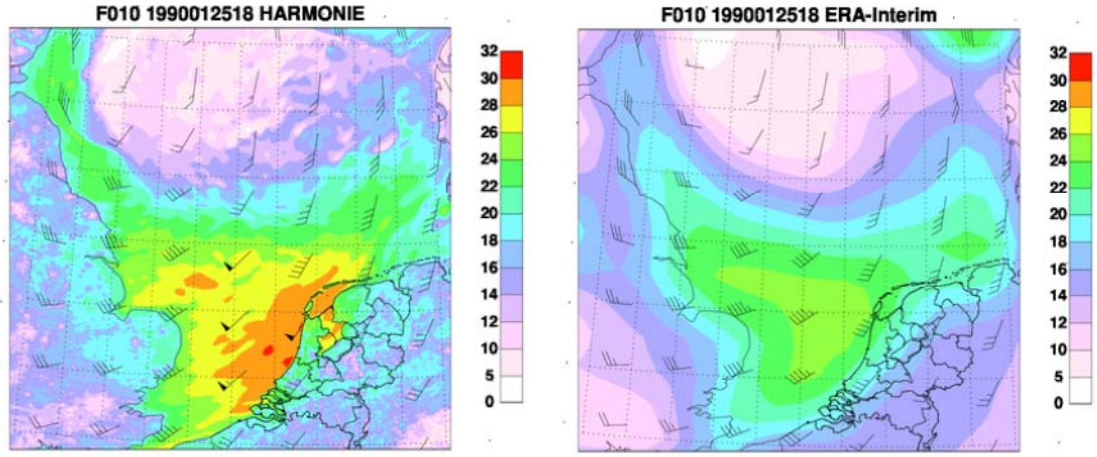

Figure 4.23. 10-m Wind fields (m/s) for HARMONIE (left) and ERA-Interim, valid at 25 Jan 1990, 18 UTC.

We calculated bias and rms error scores for HARMONIE and ERA-Interim for all stations with more than 250 data points (approximately half of the storm periods). For ERA-Interim we use values interpolated to the station location and compare these to the +006 h HARMONIE forecasts valid at the same time. For HARMONIE we follow the evaluation

procedure described in section 3.2. Given its coarse resolution, the same approach cannot be used for ERA-Interim.

As demonstrated before, Figure 4.24 shows that the HARMONIE wind fields have a slightly positive bias (note that no threshold on wind speed has been imposed). For the open-water stations the bias in ERA-Interim is generally negative. Variations between stations are larger for ERA-Interim than for HARMONIE, which is a direct consequence of the much coarser land-sea mask. The latter is probably also responsible for the overestimation of the wind speed for some land stations in ERA-Interim. For most of the stations, the rms error is clearly smaller in HARMONIE than in ERA-Interim. From this we conclude that the high resolution of HARMONIE enables a more direct evaluation with wind observations of individual stations than the coarse resolution ERA-Interim.

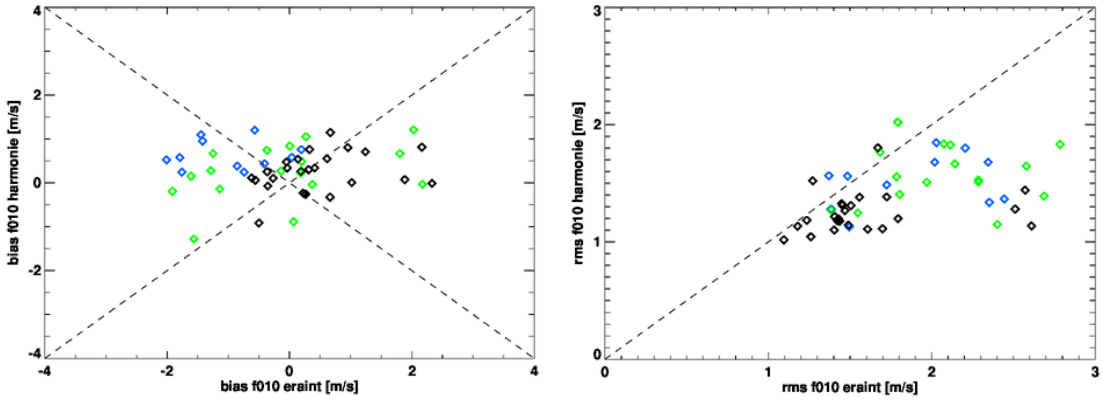

Figure 4.24. Bias (left) and rms error (right) scores of HARMONIE versus ERA-Interim for station locations. Blue points indicate open-water stations, green point stations located at the coast, and black point station located inland. The dashed lines indicate 1:1 lines (in an absolute sense).

The results presented here are in line with findings of Reistad *et al.* (2011) who performed a dynamical downscaling of the ERA-40 reanalysis dataset using the HiRLAM model. In a comparison against in-situ and satellite observation they found a significant improvement in mean values and upper percentiles of wind vectors and the significant wave height over ERA-40. Apart from the expected improvement in coastal areas, they also showed the low bias in ERA-40 had disappeared in the downscaled simulations. After dynamical downscaling the NCEP-NCAR reanalysis with a higher resolution regional model, Winterfeldt and Weisse (2009) and Winterfeldt *et al.* (2010) found only added value in coastal areas and not in the open ocean. A similar approach as in the present report was followed by Frank and Majewski (2006) who performed hindcasts of 21 historical storms that caused high surges in Northwest Germany. They conclude that high-resolution models add significant value, especially in coastal regions, and that the hindcast simulations are a suitable tool for studying extreme weather events from the past. A general overview of the benefits of using higher resolution models for downscaling global model data is presented by Feser *et al.* (2011).

5 Conclusions and follow-up steps

This report is part of the KNMI-Deltares project 'WTI2017-Wind Modelling', which aims to determine a reliable (especially above water) and detailed extreme-wind climatology for The Netherlands using a high-resolution atmospheric model (Groeneweg *et al.*, 2011). The HARMONIE model, which has a grid-spacing of 2.5 km, has been selected to perform the simulations.

5.1 Conclusions

Following the model setup described by Van den Brink *et al.* (2013), 16 storm periods, selected by Groen and Caires (2011), have been simulated with HARMONIE. Based on a verification with observations, we conclude that the wind fields produced by the model are realistic. Temporal and spatial characteristics are generally well-captured.

Given the results of the validation, the HARMONIE model set-up used for the simulation of the 16 validated storm periods will also be used for the long-term HARMONIE simulations. Any recommendations resulting from the validation in terms of hydrodynamic loads are not to be made in terms of adjusting the HARMONIE model set-up, but rather in terms of post-processing of the HARMONIE data.

Specific conclusions are listed below following the order of the report.

Atmospheric stability

- The Benschop correction factor for station locations with a measuring height different then 10 m can be applied for high wind speeds (Section 2.1.3).
- Both HARMONIE and observations show an increased (decreased) near-surface wind over open water in case cold (warm) air flows over warmer (cooler) water. In this case, the water/land wind speed ratio is increased (reduced) (Section 3.4.1).
- A comparison with two measuring masts over land and over sea indicates that HARMONIE represents the boundary layer in a realistic way. The impact of stably stratified conditions is obviously present, but the effect is too low (Section 3.4.2).

Temporal evolution

- Temporal correlation between modelled and observed wind speed is 0.95 over sea. Over land values are slightly smaller, differences between stations are small (Section 4.1.2.1).
- Over sea, modelled wind speeds show a positive bias of about 0.5 m/s. For most stations, the rms error is between 1.5 and 2.0 m/s. For wind speeds over 17.2 m/s (8 Bft and higher) these values hardly change. The bias in wind direction is a few degrees, rms scores range from 15° when all data are taken into account to order 10° for winds of 8Bft and higher. These numbers are rather similar to those derived in operation practice. Note that the observational error is about 1 m/s in the wind speed and 10° in wind direction (Section 4.1.2.1).

- Over land, differences between stations are higher. When all data is considered the wind speed bias is mostly close to zero with rms errors between 1.0 and 1.5 m/s. For wind speeds of 8 Bft and higher generally a negative bias of about 2 m/s is identified with rms errors varying from 1.5 to 4 m/s (Section 4.1.2.1).
- There is no trend in the scores for the 16 storms. For relatively small, quickly developing systems with the centre of low pressure passing close to The Netherlands the difference with observations is largest (Section 4.1.2.2).
- Hour-to-hour variations in the 10-m wind speed are reasonably captured by the model. Extreme changes are clearly underestimated (Section 4.1.2.3).

Spatial patterns

- Spatial correlation between observations valid at the same time amounts 0.87 on average. Scatterometer data gives a comparable number (Section 4.1.3.1).
- HARMONIE represents spatial gradients between a selection of stations in 10-m wind speed and surface pressure rather well (Section 4.1.3.2).
- Bias and rms error scores based on satellite winds over open water from Quikscat agree with scores derived from station observations (Section 4.1.4).
- Wind patterns over Lake IJssel are accurately reproduced by the model, including the impact of stability on the near-surface wind speed (Section 4.2).

Surface stress and relation between HARMONIE and ERA-Interim

- Over sea, surface stress is highest in areas of high wind speed, over land the opposite is true as variations in stress are mainly dominated by variations in roughness length (Section 4.3).
- Coastlines and large water bodies like Lake IJssel and the Waddensea are accurately resolved in HARMONIE, while they are only partly resolved or absent in ERA-Interim. Large-scale spatial pattern in the wind field are identical in both models. HARMONIE resolves much more small-scale structures (Section 4.4).
- The high resolution of HARMONIE enables a more direct evaluation with station observations than the coarse resolution of ERA-Interim (Section 4.4).

5.2 Follow-up steps

To establish the value of the high-resolution model for the determination of the HBCs in more detail, simulations with hydrodynamic models must be performed. This will demonstrate the added value of the high-resolution model in terms of calculated surges and wave characteristics. To be able to derive extreme winds with a return period of 10000 years, all storm periods in the ERA-Interim period (1979-2010) will be simulated with HARMONIE. In total, we have computing capacity to simulate roughly 20% of the ERA-Interim period. The long-term dataset of simulations will also be used to determine if any post-processing of the HARMONIE wind fields is required.

References

Baas, P. and De Waal, H. 2012. 'Interim report on the validation of HARMONIE', Technical Report 1204199-004-HYE-0004 Deltares.

Benschop, H., 1996. Windsnelheidsmetingen op zeestations en kuststations: herleiding waarden windsnelheid naar 10-m niveau, KNMI TR-188, 16pp.

Bottema, M., 2007. Measured wind-wave climatology Lake IJssel (NL). Main results for the period 1997-2006. Report RWS RIZA 2007.020, July 2007 (http://english.verkeerenwaterstaat.nl/kennisplein/3/5/359788/ Measured_wind-wave_climatology_lake_IJssel_(NL)-main_results_for_the_period1.pdf).

Caires, S., De Waal, H., Groen, G., Wever, N., Geerse, C., 2009. Assessing the uncertainties of using land-based wind observations for determining extreme open-water winds. SBW-Belastingen: Phase 1b of subproject "Wind modelling". Deltares report 1200264-005, October 2009.

De Rooy, W.C., Kok, K., 2004. A combined physical-statistical approach for the downscaling of model wind speed. *Weather and Forecasting*, **19**, 485-495.

De Waal, H. , 2010. Spatial wind input for HBC production runs. SBW-Belastingen. Phase 3 and conclusions of subproject "Wind modelling". Deltares Report 12000264-005 (Phase 3).

Dee, D.P, *et al.*, 2011. The ERA-Interim reanalysis: configuration and performance of the data assimilation system. *Q. J. Roy. Met. Soc.*, **137**, 553-597.

Feser, F., B. Rockel, H. von Storch, J. Winterfeldt, and M. Zahn, 2011. Regional Climate Models Add Value to Global Model Data: A Review and Selected Examples. *Bull. Amer. Meteor. Soc.*, **92**, 1181–1192.

Frank, H.P., and D. Majewski, 2006. Hindcasts of historic storms with the DWD models GME, LMQ and LMK using ERA-40 reanalysis. *ECMWF Newsletter*, **109**, 16-21.

Groen, G. and Caires, S. 2011. 'Selection of historical storms for atmospheric model validation. SBW-HB Wind modelling', Technical Report 1204199-004 KNMI/Deltares.

Grachev, A., C. Fairall, 1996. Dependence of the Monin-Obukhov Stability Parameter on the Bulk Richardson Number Over the Ocean. *J. of Appl. Meteor.*, **36**, 406-415, 1996.

Groeneweg, J., Burgers, G., Caires, S., and Feijt, A. 2011. 'Plan of approach SBW wind modelling. SBW - Belastingen', Technical Report 1202120-003 Deltares.

Groeneweg, J., Burgers, G., and Caires, S. 2012a. 'Adjusted Planning SBW Wind', Technical report RWS.

Groeneweg, J., S. Caires, and C. Roscoe, 2012b. Temporal and spatial evolution of extreme events. Proceedings of 33rd Conference on Coastal Engineering, Santander, Spain, 2012

Gryning, S.E., E. Batchvarova, B. Brümmer, H. Jørgensen, and S. Larsen, 2007. On the extension of the wind profile over homogeneous terrain beyond the surface layer. *Bound-Layer Meteor.*, **124**, 251-268.

Kudryavtsev, V.N., V.K. Makin, A.M.G. Klein Tank, J.W. Verkaik, 2000. A model of wind transformation over water-land surfaces. KNMI Scientific Report: WR2000-01, March 2000, 30 pp.

Lange, B., S. Larsen, J. Højstrup, and R. Barthelmie, 2004. Importance of thermal effects and sea surface roughness for offshore wind recource assessment. *J. Wind. Engineering Ind. Aerod.*, **92**, 959-988.

Lindenberg, 2011. A verification study and trend analysis of simulated boundary layer wind fields over Europe. PdD thesis, Helmholz-Zentrum Geesthacht, 116pp.

Lopez de la Cruz, J., A. Tijssen, and J. Beckers, 2010. The Evolution of Storms on the Wadden Sea. Deltares Report 120064-004-HYE-0012.

Loriaux, J.M., 2011. Offshore applications of Monin-Obukhov Similarity Theory. MSc Theses, Utrecht University, 81pp.

Muñoz-Esparza, D., J. van Beeck, and B. Cañadillas, 2010. Impact of turbulence modeling on the performance of WRF model for offshore short-term wind energy applications. 13th International Conference on Wind Engineering, 10-15 July 2011, Amsterdam, the Netherlands.

Nunalee, C. G., and S. Basu, 2013. Mesoscale modeling of low-level jets over the North Sea. Wind Energy: Proceedings of the Euromech Colloquium, edited by J. Peinke et al., Under Review.

Peña, A., T. Mikkelsen, S.E. Gryning, C.B. Hasager, A.N. Hahmann, M. Badger, I. Karagali, and M.I. Courtney, 2012. Offshore Vertical Wind Shear, Final report on NORSEWInD's work task 3.1. DTU Wind Energy-E-Report-0005(EN), August, 2012.

Portabella, M., and A. Stoffelen, 2009. On scatterometer ocean stress. *J. Atm. Ocean Tech.*, **26**, 368-382.

Portabella, M., A. Stoffelen, W.Lin, A. Turiel, A. Verhoef, J. Verspeek, and J. Ballabrera-Poy, 2012. Rain effects on ASCAT-retrieved winds: toward an improved quality control. *Trans. Geosc. Remote Sensing*, **50**, 2495 – 2506.

Reistad, M., Ø. Breivik, H. Haakenstad, O. J. Aarnes, B. R. Furevik, and J.-R. Bidlot, 2011. A high-resolution hindcast of wind and waves for the North Sea, the Norwegian Sea, and the Barents Sea. *J. Geophys. Res.*, **116**, C05019.

Royal Netherlands Meteorological Institute, 2001. Handboek Waarnemingen, http://www.knmi.nl/samenw/hawa/.

Sathe, A., S.E. Gryning, and A. Peña, 2011. Comparison of the atmospheric stability and wind profiles at two wind farm sites over a long marine fetch in the North Sea. *Wind Energy*, **14**, 767-780.

Seity, Y., Brousseau, P., Malardel, S., Hello, G., Bénard, P., Bouttier, F., Lac, C., Masson, V., 2011. The AROME-France convective-scale operational model. *Mon. Wea. Rev.*, **139**, 976-991.

Tammelin, B. *et al.*, 2011. Production of the Finnish wind atlas. *Wind energy*, **16**, 19-35.

Van den Brink, H., P. Baas, and G. Burgers, 2013: Towards an approved model set-up for HARMONIE.

Verkaik, J.W., 2001. Documentatie wind metingen in Nederland. KNMI, January 2001.

Verkaik, J.W., 2006. Downscaling of weather model forecasts. *On wind and roughness over land*, PhD thesis, Wageningen University, 69-92.

Vogelzang, J., A. Stoffelen, A. Verhoef, and J. Figa-Saldaña, 2011. On the quality of high-resolution scatterometer winds. *J. Geophys. Res.*, **116**, C10033.

Waterwet 2009, www.helpdeskwater.nl/onderwerpen/wetgeving-beleid/waterwet.

Weill, A., Eymard, L., Caniaux, G., Hauser, D., Planton, S., Dupuis, H., Brut, A., Guerin, C., Nacass, P., Butet, A., Cloche, S., Pedreros, R., Durand, P., Bourras, D., Goirdani, H., Lachaud, G., and Bouhours, G. 2003. Toward a better determination of turbulent airsea fluxes from several experiments. *J Climate*, **16**, 600–618.

Weisse, R., H. von Storch, and F. Feser, 2005. Northeast Atlantic and North Sea Storminess as Simulated by a Regional Climate Model during 1958–2001 and Comparison with Observations. *J. Climate*, **18**, 465-479.

Weisse, R., et al., 2009. Regional meteorological-maritime reanalysis and climate change projections. *Bull. Amer. Meteor. Soc.*, **90**, 849-860.

Wever, N, Groen, G., 2009. Improving potential wind for extreme wind statistics. KNMI Scientific Report: WR2009-02, March 2009.

Winterfeldt, J., and R. Weisse, 2009. Assessment of Value Added for Surface Marine Wind Speed Obtained from Two Regional Climate Models. *Mon. Wea. Rev.*, **137**, 2955-2965.

Winterfeldt, J., B. Geyer, and R. Weisse, 2010. Using QuikSCAT in the added value assessment of dynamically downscaled wind speed. *Int. J. Climatol.*, **31**, 1028-1039.